Геология и геофизика, 2021, т. 62, № 7, с. 988—1009

УДК 553.982(514)

НЕФТЕГАЗОВЫЕ КОМПЛЕКСЫ ЗОН С СЕТЬЮ РАЗЛОМОВ В РАЙОНЕ ДУНХЭТАН (*Табэйское поднятие, Таримский бассейн, Северо-Западный Китай*) И ИХ ЗНАЧЕНИЕ ДЛЯ РАЗВЕДКИ УГЛЕВОДОРОДОВ

Ц. Лю[1,2], Х. Сюй[1], Ч. Лэй[3,4], Ч. Ли[5], Ю. Сюн[5], С. Ли[5], Б. Ло[5], Д. Чень[5]

[1]*Department of Geoscience, China University of Petroleum (Beijing), Beijing, 102249, China*

[2]*Institution of Petroleum Exploration and Development of SW Tarim Basin, Tarim Oilfield Company, PetroChina, Korla, 841000, China*

[3]*Jiangxi Engineering Laboratory on Radioactive Geoscience and Big Data Technology, East China University of Technology, Nanchang, 330013, China*

[4]*Jiangxi Engineering Technology Research Center of Nuclear Geoscience Data Science and System, East China University of Technology, Nanchang, 330013, China*

[5]*Research Institution of Petroleum Exploration and Development, Zhongyuan Oilfield Company, Sinopec, Puyang, Henan, 457300, China*

Механизм образования углеводородов и нефтегазоперспективные объекты в обломочных толщах Табэйского поднятия в Таримском бассейне рассмотрены на основе комплексных сейсмических, скважинных, керновых и геохимических данных с использованием теории нефтегазовых комплексов зон с сетью разломов. Коллекторы в районе Дунхэтан являются типичными аллохтонными нефтегазовыми комплексами, приуроченными к сети разломов, с удаленными источниками углеводородов (УВ). В районе исследования выявлены две системы с сетью разломов: (1) песчаниковый коллектор Дунхэ и пермотриасовые толщи и (2) пласты J_{IV} и J_{III} в юрских толщах. Анализ корреляций между УВ и их источником показал, что нефтегазовый комплекс юрской толщи является производным каменноугольного песчаного коллектора Дунхэ. Системы сетей разломов подразделяются на четыре структурных типа: (1) зона, соединенная разломами с материнскими породами, (2) разлом—несогласие—зона временного хранилища УВ, (3) разлом—зона временного хранилища УВ—несогласие, (4) зона временного хранилища УВ—разлом. По характеристикам нефтегазовых комплексов зон с сетью разломов коллекторы подразделяются на 15 типов и три группы: верхнее, внутреннее и нижнее (приграничное) временные хранилища углеводородов. Комплексный анализ генерации УВ и времени образования разломов выявил четыре периода накопления УВ в коллекторах, при этом на первых трех этапах происходило накопление нефти, а на последнем — газа. Район исследований характеризуется многократными стадиями формирования коллекторов и перестройки сетей разломов в них, что является основной причиной различия углеводородного состава их вертикальных блоков. Разрывно-блоковые коллекторы и литологические коллекторы, служащие внутренними и верхними хранилищами УВ, являются основными нефтегазопоисковыми объектами в обломочных толщах в области исследования.

Удаленное от источника накопление углеводородов, нефтегазовые комплексы зон сетей разломов, многократное накопление и перестройка коллектора, Табэйское поднятие, Таримский бассейн, Северо-Западный Китай

FAULT MESH PETROLEUM PLAYS IN THE DONGHETANG AREA, TABEI UPLIFT, TARIM BASIN, NW CHINA, AND THEIR SIGNIFICANCE FOR HYDROCARBON EXPLORATION

Q. Liu, H. Xu, Z. Lei, Z. Li, Y. Xiong, S. Li, B. Luo, D. Chen

The hydrocarbon formation mechanism and potential targets in clastic strata from the Tabei Uplift, Tarim Basin, are documented using the fault mesh petroleum plays theory, based on integrating seismic, well log, well core and geochemistry data. The reservoirs in the Donghetang area are typical allochthonous and far source fault mesh petroleum plays. There are two sets of fault meshes in the study area: (1) the Donghe sandstone and combination of Permian and Triassic strata and (2) combination of the J_{IV} and J_{III} formations in the Jurassic strata. The fault mesh petroleum play in the Jurassic is a secondary reservoir that originates from the Carboniferous Donghe sandstone reservoir adjustment based on source correlation. The fault mesh carrier systems are divided into four styles according to the fault mesh architecture: (1) fully connected, (2) fault–unconformity–transient storage relay, (3) fault–transient storage–unconformity relay, and (4) transient storage–fault relay. According to the characteristics of the fault mesh petroleum plays, the reservoirs are of 15 types and form three categories: upper transient storage, inner transient storage, and margin-transient storage. Integrated analysis of the hydrocarbon generation and faulting time periods reveals that there were four periods of hydrocarbon charging, with

✉e-mail: oasis_1996@63.com

DOI: 10.15372/GiG2020125

the first three stages charging the reservoirs with oil and the last stage charging the reservoirs with gas. There are multiple stages of reservoir accumulation and adjustment in the fault mesh in the study area. These multiple stages of fault mesh accumulation and adjustment are the main reason that the multiple vertical units of the reservoirs have different hydrocarbon properties. Fault-block reservoirs and lithologic reservoirs related to the inner transient storage and upper transient storage styles are the main exploration targets in the clastic strata in the study area.

Allogenic and far source accumulation, fault mesh petroleum plays, multiple accumulation and adjustment, Tabei Uplift, Tarim Basin, NW China

INTRODUCTION

Dow first proposed the 'oil system' concept in 1972 (Dow, 1972), and related concepts were subsequently described (Dow, 1974; Perrodon, 1983, 1992; Demaison, 1984; Meissner, 1984; Ulmishek, 1986; Magoon, 1988, 1992). This work gave birth to the 'petroleum system' concept that was described in the AAPG Memoir 60 (Magoon and Dow, 1994). A 'petroleum system' comprises a pod of mature source rock and all of the migration paths, reservoir rocks, caprocks, and traps that can be charged by that source rock to produce oil and gas accumulations.

The Chinese geologists who applied the concepts of the petroleum system found that it was not suitable for hydrocarbon exploration in the complex superimposed basins in northwestern China (Pang et al., 2003, 2010). Some studies proposed the source control theory (Hu, 1986) and hybrid petroleum systems (Zhao and He, 2000), according to the reservoir formation characteristics in the superimposed basins. Jin and Wang (2004) described the concept of a petroleum accumulation system, which uses the reservoir as a key unit of study. The concept of the petroleum accumulation system emphasizes that reservoir formation relies on efficient allocation of all of the hydrocarbon formation units to form a reservoir. Xu et al. (2008) divided the petroleum accumulation system into three types following the origin of a source–reservoir–cap and its assemblage, which include allogenic, authigenic, and hybrid hydrocarbon source petroleum accumulation systems.

Zhang et al. (2003, 2004) proposed the concept of fault mesh petroleum plays based on research on reservoir-forming processes of secondary reservoirs in the Jiyang Depression, Bohai Bay Basin, eastern China. A well-defined fault mesh petroleum play usually contains three basic elements, a hydrocarbon source network at the base, a transient storage for migrating hydrocarbons in the middle, and a petroleum accumulation network at the top (Zhang et al., 2003, 2004). The mesh that contains the oil source network at the base consists of primary faults and (or) regional unconformities in direct contact with mature hydrocarbon source beds and secondary faults that cut lenticular sandstones. The transient storage is a sheetlike, thick, porous sandstone deposit. The fault mesh petroleum play is the allogenic hydrocarbon that was generated in the lower strata and migrated through the oil source network, temporarily accumulated in the transient storage, and migrated once more vertically or laterally into shallower reservoirs. Such a play concept stresses the role of faults in the transmission of petroleum fluids from relatively deeply buried source rocks to suitable petroleum host rocks and traps in the stratigraphically younger strata (Wang et al., 2005). The accumulation processes of fault mesh petroleum plays were proven by physical simulations (Zhang et al., 2003, 2004). Zhang et al. (2013) divided the fault mesh petroleum plays into far-source and near-source styles according to the relationship between the petroleum accumulation system and the source rock.

Many studies have focused on the reservoir formation in the Tabei Uplift, Tarim Basin, for oil source correlation, hydrocarbon accumulation stages, and reservoir formation mechanisms (Li et al., 1996; Zhang et al., 2000; Zhu et al., 2013a,b; Li et al., 2016). There are two viewpoints on the origin of the Jurassic condensate reservoirs in the study area: Zhang et al. (2012) suggested that the condensate reservoirs are hybrids from marine and continental hydrocarbons, and Liang et al. (1998) suggested that the condensate reservoirs originated from marine hydrocarbons, which resulted from hydrocarbon adjustment. Commonly, the Carboniferous and Jurassic reservoirs were studied as separate petroleum accumulation systems, and the reservoir formation mechanism from local to regional scale is rarely discussed. This study applies the fault mesh petroleum play theory to analyze the reservoir formation mechanism and accumulation patterns during hydrocarbon generation periods, faulting stages, and transient storage and to predict exploration targets and beneficial zones in the study area.

DATA AND METHODS

Seismic attributes from the seismic data in the depth domain were analyzed to understand the reservoir distribution of the transient storage and petroleum accumulation network during the Jurassic. Cored material of 2686 and 180 samples in the Donghe sandstone and Jurassic strata, respectively, were used to analyze the petrophysical properties of the transient storage and petroleum accumulation network. The architecture of the un-

conformity complex between the Jurassic and lower strata was determined by well correlation. Geochemistry parameters and light hydrocarbon compositions from 11 wells from the Donghe sandstone and six wells from the Jurassic strata were used to analyze the source relationship between the Donghe sandstone and Jurassic reservoirs, which determined the *n*-alkanes distribution and light hydrocarbon composition.

Gas compositions were measured using an Agilent 7890 gas composition instrument, which was equipped with four valves, six packed columns, a flame ionization detector (FID), and two thermal conductivity detectors (TCD). The oven temperature was held at 50 °C, and the FID temperature remained at 80 °C.

The gas chromatography (GC) was performed using an Agilent 6890A equipped with a fused silica column (HP-PONA, 50 m × 0.20 mm, i.d. ×0.5 mm film thickness) and an FID at 300 °C. The experimental methods of the GC were described in detail by Song et al. (2016). The urea complexation method was used to separate the *n*-alkane and UCM from the oil-saturated hydrocarbons.

The bulk composition: The oil was extracted by washing the oil sand with chloroform, and the bulk composition, including alkane, asphalt, aromatic, and resin, was separated using silica gel column chromatography.

The 2DMove software was used to balance two cross sections and analyze fault evolution processes and timing of the Paleozoic faults. Flexural slip was used to maintain stratigraphic thickness, and fault parallel flow was used during fault restoration.

GEOLOGIC SETTING

The Tarim Basin lies between the Chinese Tianshan Mountains to the north and western Kunlun Mountains to the south and is confined by the Altun Mountains to the southeast (Fig. 1, A, B). The Tabei Uplift is located between the Kuche and Manjiaer depressions in the Tarim Basin. The Donghetang tectonic belt is located at the northern Halahatang sag, in the middle of the Tabei Uplift (Fig. 1, C). It consists of five Carboniferous Donghe sandstone reservoirs (DH1, DH4, DH5, DH6, and DH14) and a Jurassic condensate reservoir (Fig. 1, D).

PETROLEUM GEOLOGIC SETTING

The strata from Ordovician through Quaternary were drilled in the study area. Figure 2 shows the sedimentary basin fill and stratigraphic framework in the study area. The Donghe sandstone is a diachronous unit that spans the Devonian–Carboniferous (Wang et al., 2004). We use the term "Carboniferous Donghe sandstone" in this paper for convenience. There is an onlapped unconformable surface with the Silurian at the bottom and a truncation unconformable surface with the Permian and Jurassic at the top of the section.

The Donghe sandstones of the DH1 reservoir in burial history are characterized by long-term subsidence to a shallow depth and short-term subsidence to a large depth (Fig. 3). It was uplifted to the surface and eroded in the late Hercynian time. The subsidence continued in the Early Cretaceous. Then, fast subsidence to the present buried depth range from 5700 to 6000 m took place in the Hiyama time. The reservoir temperature from the DH1 well in the Donghe sandstones at 5718 m is 140 °C.

The previous work suggests that in the study area, the Donghe sandstone deposits in a shoreline environment and is a thick fine-grained quartz sandstone (Li et al., 2016). The average thickness of the Donghe sandstone is approximately 250 m and can be divided into ten sand sets on the basis of analyzing sequence stratigraphy (Fig. 2). The hydrocarbon source rocks are Ordovician marine carbonate rocks from the southern Manjiaer Depression (Zhang et al., 2000; Chang et al., 2013).

The Jurassic and its contact with older strata form a high-angle unconformity and a parallel unconformity with the Cretaceous. The Lower Jurassic can be divided into two formations, which include the J_{IV} and J_{III}, from bottom to top. The sedimentary depositional system of the J_{IV} formation is a braided river environment, and it is distributed widely in the study area (Fig. 4, C). The J_{III} formation was deposited by an alluvial fan and is distributed in the northern and northwestern parts of the study area (Fig. 4, D).

The regional seal includes a Carboniferous bioclastic limestone and mudstone assemblage and a thick lacustrine mudstone in the Middle–Upper Jurassic. There are two petroleum accumulation assemblages: The lower assemblage is a Carboniferous Donghe sandstone, bioclastic limestone and mudstone, and the upper assemblage comprises the J_1 and $J_{2\text{-}3}$ formations. The reservoir properties are significantly different between the lower and upper assemblages, with the former being a crude oil reservoir, and the latter a condensate reservoir.

STRUCTURE EVOLUTION

There are two fault systems in the study area: a thrust and strike-slip fault system that was active in the Paleozoic and an extensional fault system active in the Mesozoic and Cenozoic. The thrust faults strike in a NE–SW direction, and the strike-slip faults are right-lateral and strike in a NW–SE direction (Fig. 1, D). The normal fault system in the Jurassic consists of echelon faults in a NE direction (Fig. 1, F).

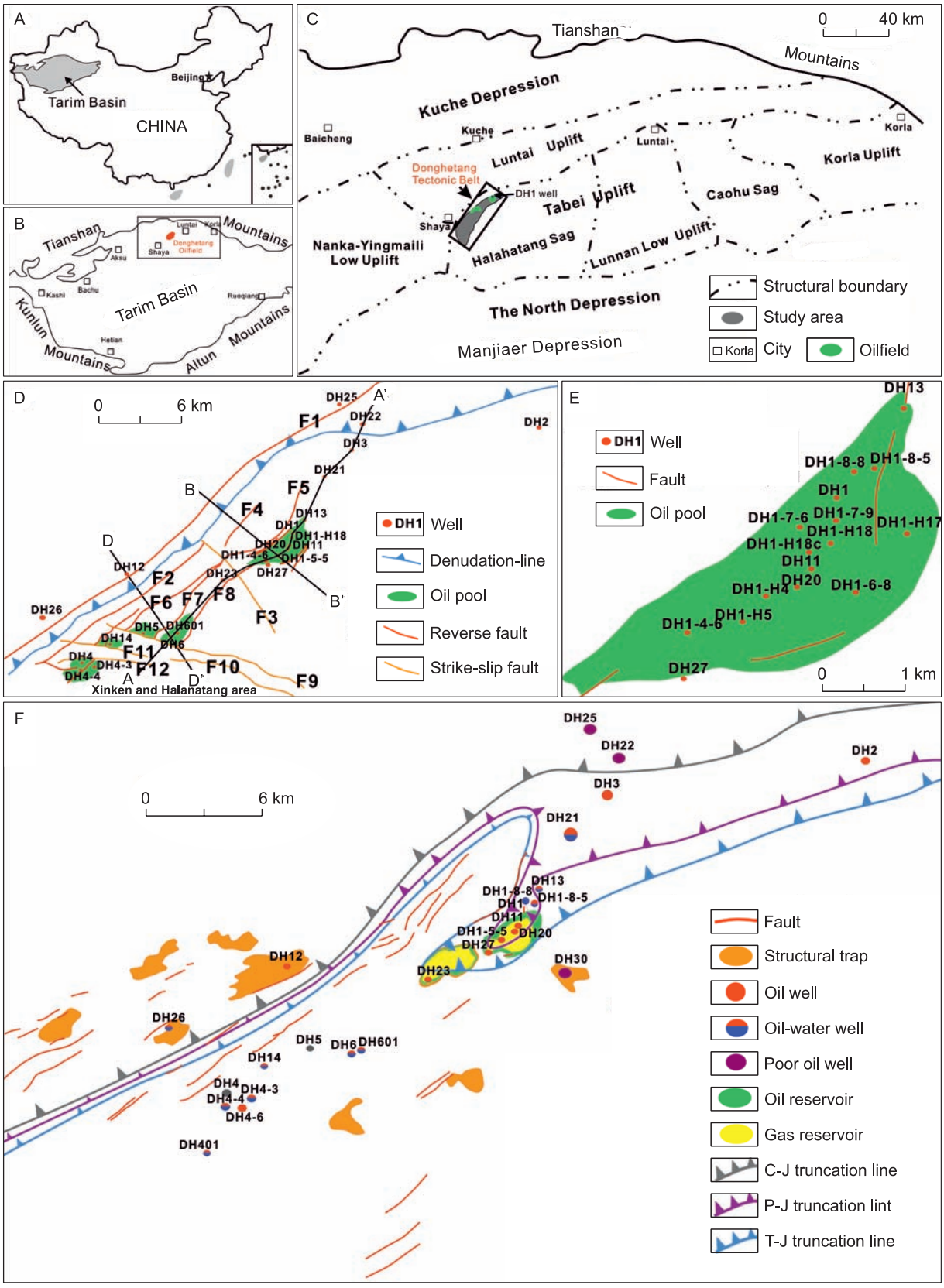

Fig. 1. Geological setting of the Donghetang area petroleum plays.

A, B, and C are the structural locations of the Tarim Basin, Tabei Uplift, and Donghetang tectonic belt, respectively, and D is the fault system in the Carboniferous Donghe sandstone. E is the well location in the DH1 oilfield, and F is the fault system in the Jurassic.

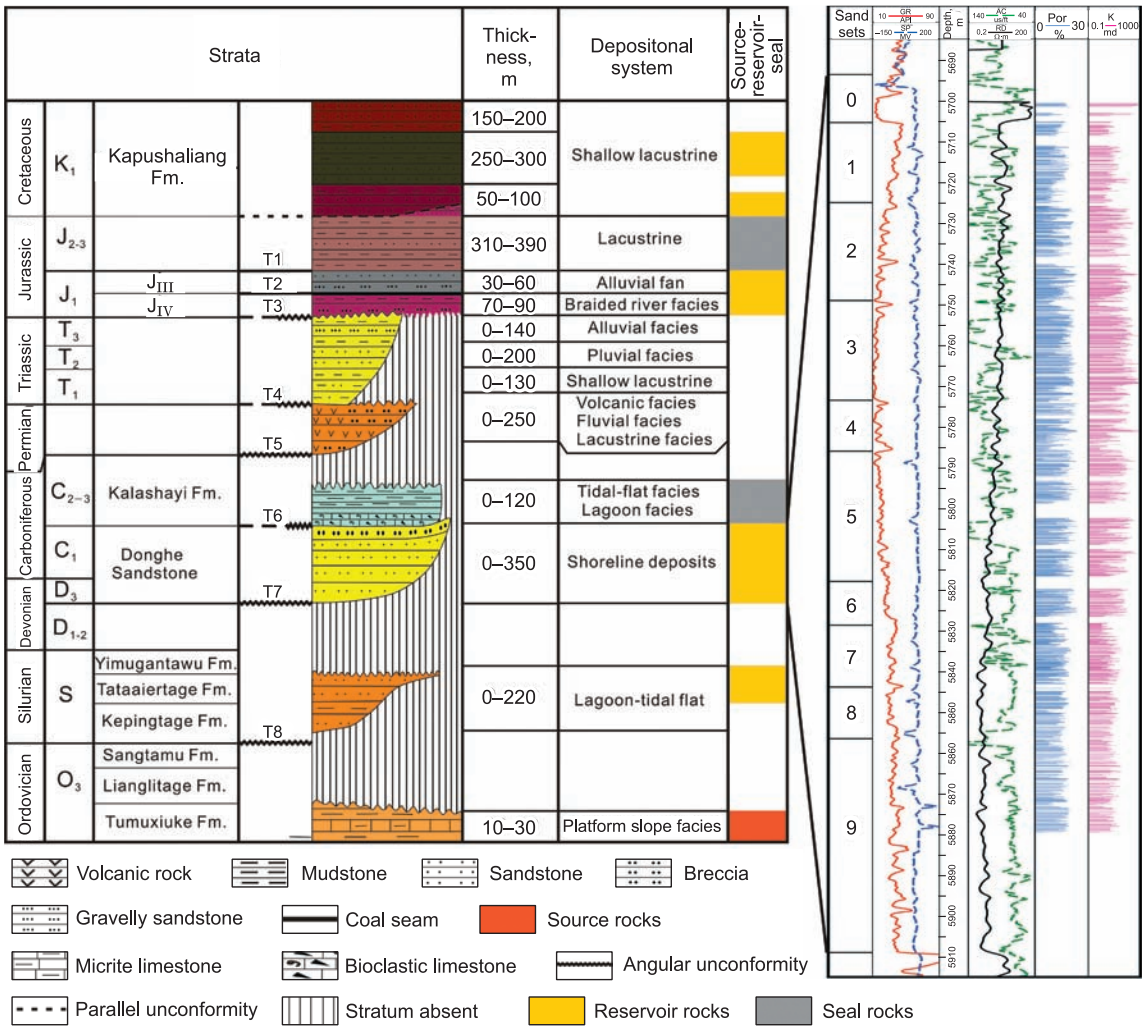

Fig. 2. The geological column of the Donghetang area and the petrophysical properties of the Carboniferous Donghe sandstone in the DH11 well core section, from the well core data.

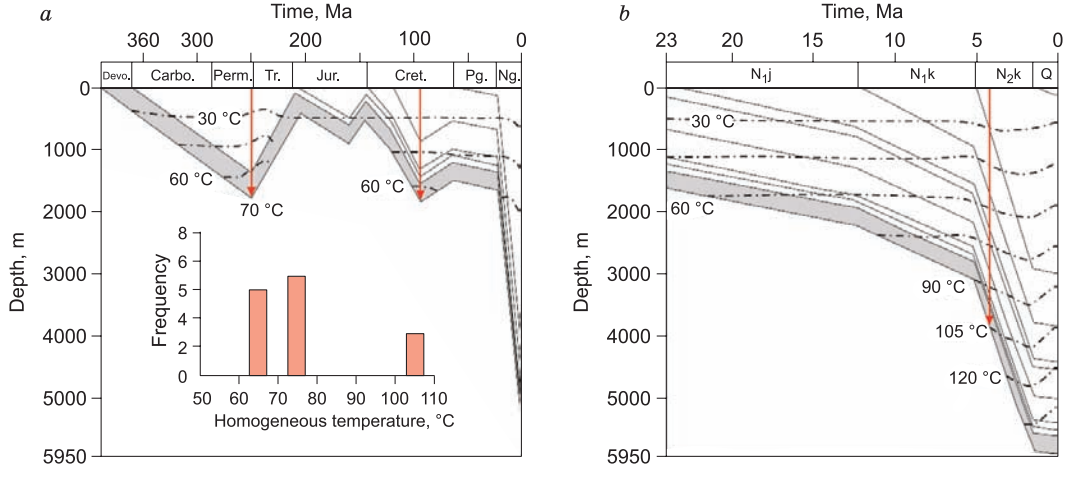

Fig. 3. The depth–thermal history and hydrocarbon charging periods of the Donghe sandstones reservoir, DH1 oilfield, and the gray rectangle marks the Donghe sandstones.

The histogram of homogeneous temperature of salt-water inclusions associated with hydrocarbon inclusion in the DH11 well is after Zhang et al. (2012) (*a*). The Neogene of hydrocarbon charging is after Zhang and Luo (2012) (*b*), who used the K–Ar dating of authigenic illite of Carboniferous sandstone reservoirs in the Ha 6 well from the Halahatang sag.

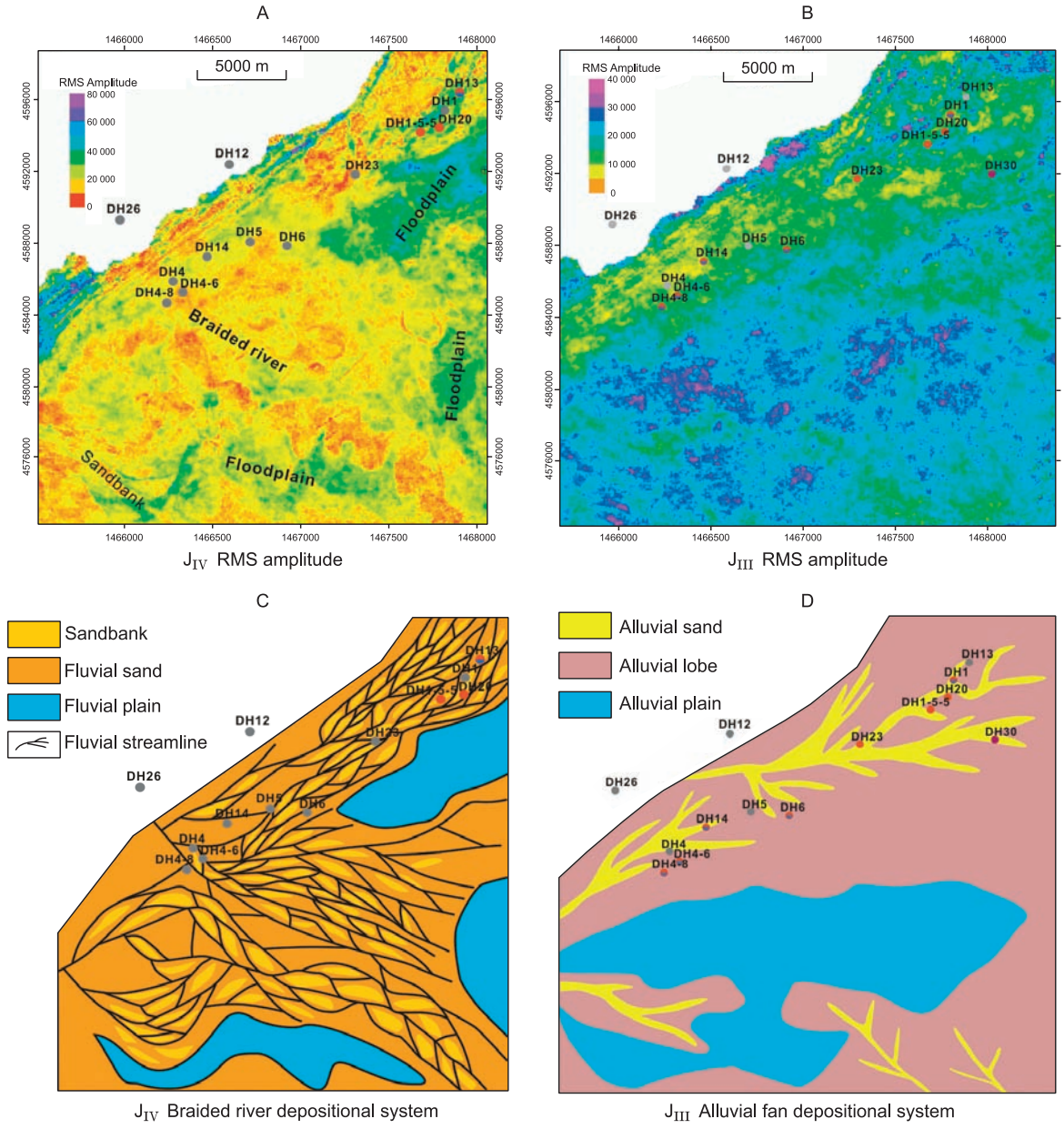

Fig. 4. The RMS amplitude of the J_{IV} and J_{III} formations and its interpretation. Partial hydrocarbons are in the wells distributed in the J_{IV} and J_{III} formations. The legend of the hydrocarbon well is shown in Fig. 1, F.

The ancient uplift formed in the early Hercynian time, and the fault activity reached a maximum during the middle to late Hercynian (Tang et al., 1999). Volcanic activity occurred in the Permian to the Early Triassic, and the Paleozoic structural framework was set in the Late Triassic (Liu et al., 2012). The F1 and F5 faults (Fig. 5) were still active in the Jurassic to Cretaceous owing to the strong activity of the Tianshan thrust fault zones (Tang et al., 2012). The extensional fault system formed in the Neogene because of the earlier Kuche foreland frontal uplift in the northern part of the study area (Wei et al., 2001).

Generally, during the Devonian–Triassic, there was an intense thrust and uplift stage. Fault activity reached the maximum during the Permian–Triassic, which is why Permian and Triassic strata were eroded. The study area began to subside in the Jurassic, which resulted in a regional high-angle unconformity between the Jurassic and older strata (Fig. 1, F). There was weak thrust activity during the Jurassic–Cretaceous. The thrust faults in the Paleozoic were reactivated by negative inversion during the Eocene–Miocene (Chen et al., 1998;

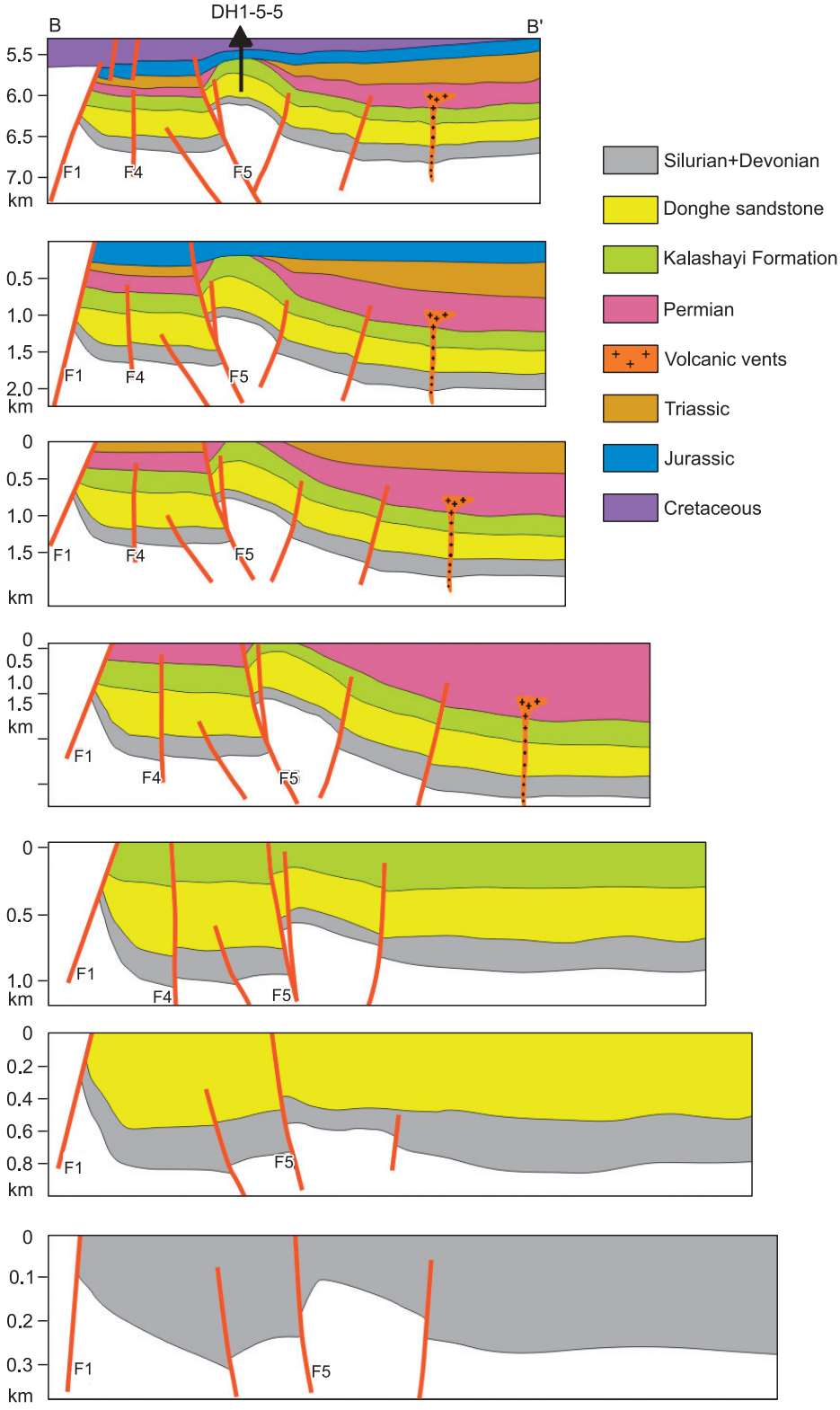

Fig. 5. The structural evolution of the Line B–B′. The profile location and fault numbers are shown in Fig. 1, D.

Tang et al., 1999; Cheng et al., 2009). During this final stage, the strata inclination in the study area experienced inversion owing to the subsidence of the northern Kuche Depression. It resulted in a structural high that migrated from north to south, affecting the Jurassic and its overlying strata (Fig. 5).

RESULTS

The characteristics of fault mesh. The transient storage

The petrophysical properties of the Donghe sandstone reservoir in middle sand sets 2 to 5 with permeabilities four to eight times higher than at both ends, but little change in porosity, according to an analysis of 2686 samples from well cores (Fig. 6, A). The permeability in sand sets 0 to 8 is 1–50 md, 0.4–200 md, 0.1–400 md, 0.4–500 md, 0.4–300 md, 0.2–700 md, 0.5–250 md, 0.2–70 md, and 0.1–20 md, respectively, and the average is 31.4, 15.6, 88.1, 167.3, 79.5, 93.65, 38.98, 8.82, and 8.91 md, respectively. The average porosity is 15%, and the range is from 3 to 21% in the Donghe sandstone. The average permeability is 360 md, and the average porosity is 18.6% in the J_{IV} formation, according to an analysis of 42 samples from well core data (Fig. 6, B).

The transient storage occurred over a relatively large geographic area in a porous, well-connected, and thick sheetlike sandstone reservoir (Zhang et al., 2003, 2004). These sandstones serve as temporary storage spaces, through which deep-sourced petroleum fluids migrate, either laterally or vertically, into shallower reservoirs (Zhang et al., 2003, 2004). However, the concept of fault mesh petroleum plays was proposed under the geologic setting of shallow burial depth (less than 2000 m) and high petrophysical properties (with an average porosity of 35.3% and a permeability of 1500 md) compared to those of deeply buried reservoirs (below 5000 m) with low petrophysical properties. At the same time, following Zhang et al. (2003, 2004), the key for hydrocarbon accumulation of that system is the well-developed transient storage, which is widespread and consists of sheetlike, thick, well-connected porous sandstone deposits. According to that concept, there are two sets of transient storage reservoirs in the study area: the shoreline facies of the Carboniferous Donghe sandstone reservoir (average thickness of 250 m) and braided river deposits of the J_{IV} formation, a sandstone reservoir with an average thickness of 10 m (Fig. 7).

The petroleum accumulation network

The petroleum accumulation network above the transient storage provides suitable reservoirs for hydrocarbon accumulation (Zhang et al., 2003, 2004). There are two sets of petroleum accumulation networks: continental deposits from Permian to Triassic and alluvial fan deposits in the J_{III} formation. The average permeability is 45 md, and the average porosity is 16.5% in the Jurassic petroleum accumulation network of the J_{III} formation, according to 138 samples from the well core (Fig. 7). No hydrocarbons have been found in the Permian–Triassic in the drilled wells, and the hydrocarbon distribution widely in the J_{III} formation according to the well-logging interpretation and well test (Fig. 4, D). The thin sandstone reservoirs in the thick lacustrine mudstone of J_{2-3} might also be part of the petroleum accumulation network.

The hydrocarbon source network

The hydrocarbon source network provides fairways for hydrocarbons generated in a deep source to migrate vertically upward to shallow strata and often consists of primary faults and/or regional unconformities in direct contact with mature petroleum source beds and secondary faults intercepting lenticular fluvial sandstones

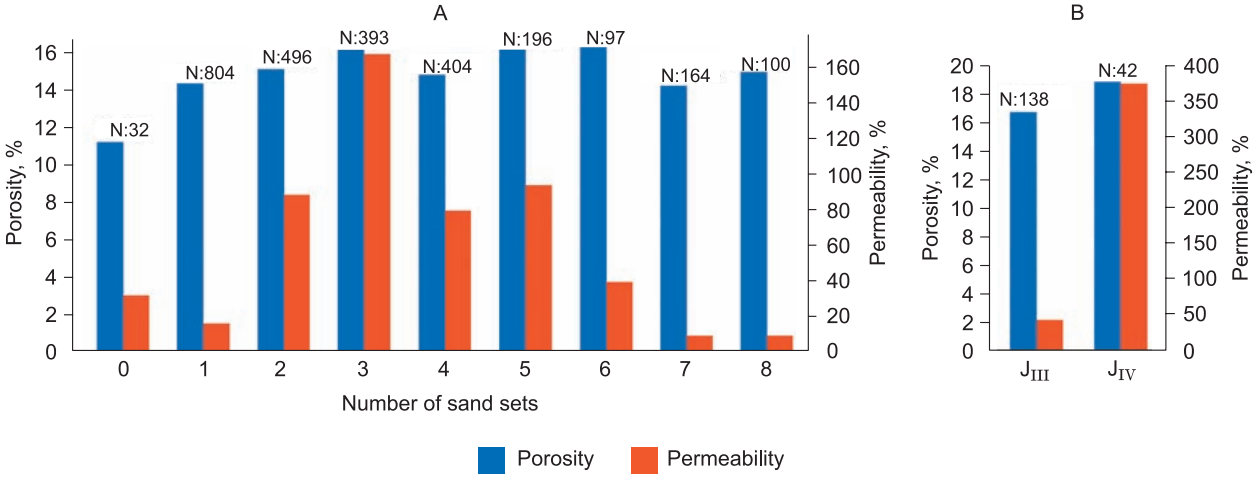

Fig. 6. The petrophysical properties of the transient storage and the petroleum accumulation network.

A is the average petrophysical properties in the different sand sets of the Donghe sandstone, and B is the average petrophysical properties in the J_{IV} and J_{III} formations. N is the sample number.

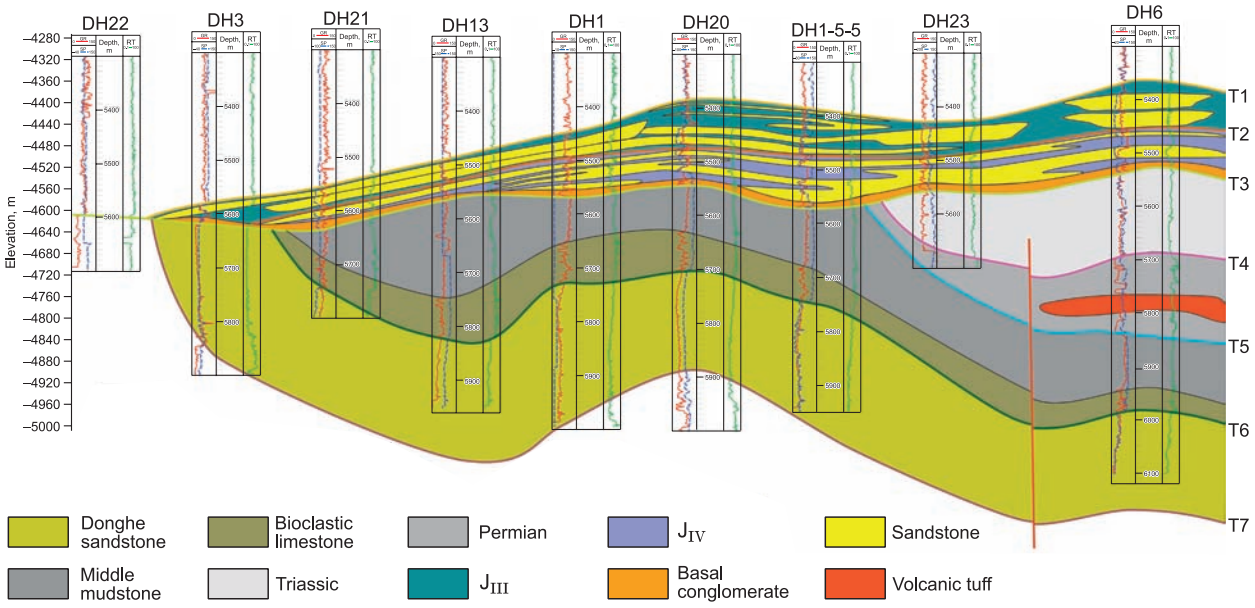

Fig. 7. The characteristics of the reservoir rock connectivity in the transient storage and the petroleum accumulation network in the study area.

The transient storage of the Carboniferous Donghe sandstone is between T6 and T7, and the transient storage of the J_{IV} formation is between T2 and T3. The petroleum accumulation network of the J_{III} formation is between T1 and T2. There is a basal conglomerate with a thickness of 3 to 5 m above the unconformity contact between the Jurassic and older strata. The well location is shown in Fig. 1, D.

(Zhang et al., 2004). The hydrocarbon source rocks are Ordovician marine source rocks in the southern study area of the Manjiaer Depression (Zhu et al., 2013; Huang et al., 2016). The hydrocarbon accumulation in the Carboniferous Donghe sandstone and Jurassic reservoirs that originated from the Ordovician source rocks must have migrated through the hydrocarbon source network.

The hydrocarbon source network demonstrates full-connection and low-connection styles according to the time–space relationships between the faults, unconformity, and two sets of transient storage units in the study area. The fully connected style of the hydrocarbon source network means that the two sets of transient storage are connected with the hydrocarbon source rocks by faults, an unconformity, and/or a sandstone reservoir (Fig. 8). The low-connection style of the hydrocarbon source network means that just the transient storage of the Carboniferous Donghe sandstone is connected with the hydrocarbon source rocks by faults and/or an unconformity, and the second transient storage is not connected with those faults and/or unconformity (Fig. 8).

The faults that have been active for a long time in the northern study area, such as faults F5 and F1, and the unconformity between Jurassic and Carboniferous, constitute the fully connected style of the hydrocarbon source network. The faults that formed during the Carboniferous–Triassic constitute the low-connection style of the hydrocarbon source network and are primarily distributed in the middle part of the study area.

The small-scale extensional faults in the Jurassic are not directly connected with the Ordovician source rocks, but can serve as hydrocarbon migration channels for the petroleum accumulation network of the J_{III} formation. The hydrocarbon from the J_{IV} reservoirs and Carboniferous Donghe sandstone reservoirs migrated along extensional faults to the J_{III} formation and accumulated.

Physical properties and geochemical composition of crude oil

The reservoirs of the Carboniferous Donghe sandstone and Jurassic include crude, heavy, and condensate oil. The Donghe sandstone reservoir and the Jurassic reservoir are similar in the crude oil density, viscosity, sulfur content, and saturated hydrocarbon content, which are 0.76 to 0.92 g/cm^3, 5 to 13 mPa·s, 0.2 to 1%, and 25 to 72%, respectively. The viscosity of the condensate reservoir in the Jurassic ranges from 0.8 to 1.5 mPa·s. The ratio of the saturated to aromatic hydrocarbons in the Donghe sandstone reservoir ranges from 2 to 7 and from 1.6 to 2.8 in the Jurassic reservoir (Table 1).

The value of the odd–even predominance (OEP) and carbon preference index (CPI) is approximately 1. The values of Ph/nC_{18} and Pr/Ph in the Donghe sandstone and Jurassic reservoir are similar, ranging from 0.35

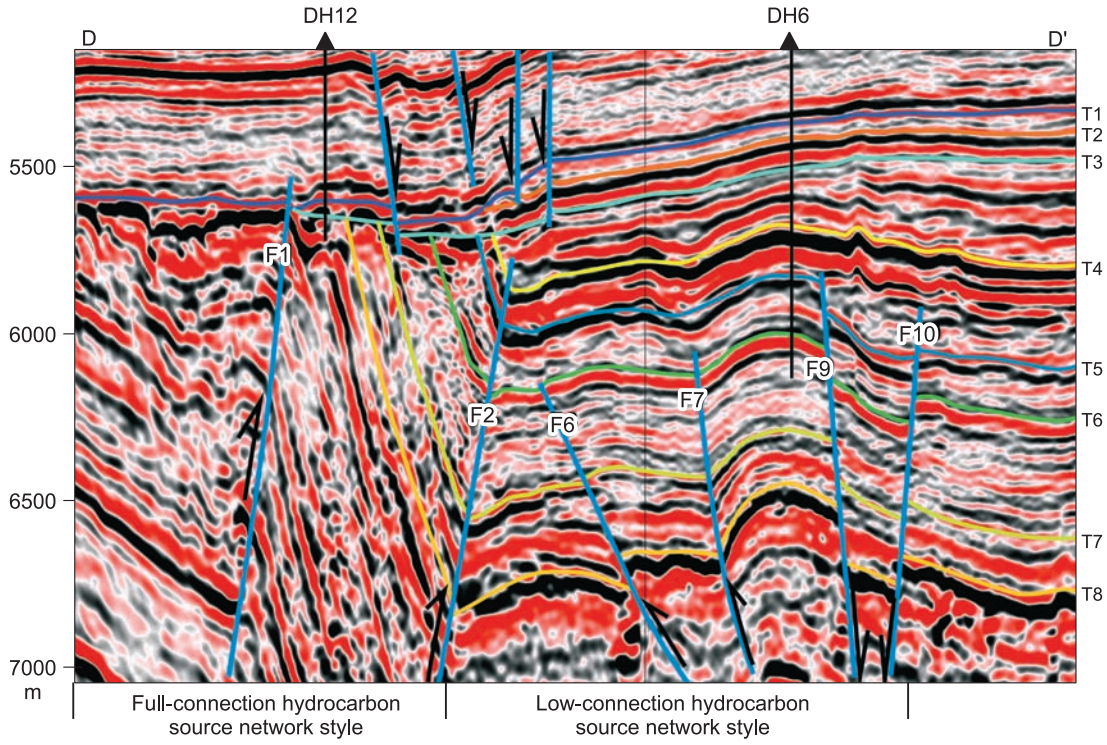

Fig. 8. The style of the hydrocarbon source network in the seismic section. The Ordovician source rocks are located below T8. The section line D–D′ and well location are shown in Fig. 1, D.

to 0.7 and less than 1, respectively. The value of Pr/nC_{17} ranges from 0.3 to 0.8 in the Donghe sandstone reservoir and from 0.2 to 0.4 in the Jurassic reservoir (Table 2).

The natural gas composition and light hydrocarbon composition

The Donghe sandstone natural gas is characterized by high CO_2 and N_2 contents and high relative density: between 18 and 32%, 20 and 36%, and 0.8 to 1.2, respectively. The Jurassic is naturally characterized by high methane content and a low relative density, between 82 and 87% and less than 0.7, respectively (Table 3).

The Donghe sandstone and Jurassic reservoir have similar contents of *n*-alkanes and aromatics in the light hydrocarbon composition, 35 to 50% and 0.3 to 16%, respectively. The contents of the isoalkane and cycloalkane in the Jurassic reservoir are high, 26 to 36% and 9 to 19%, respectively. The contents of those in the Donghe sandstone reservoir are low, 12 to 31% and 0.2 to 15%, respectively (Table 4).

DISCUSSION

The origin of the Donghe sandstone and Jurassic hydrocarbon

Mango (1987, 1990) suggested that the K1 values of hydrocarbons in the same source are basically consistent, and the K1 value is defined as the ratio of sum of concentrationsof (2-methylhexane+2,3-dimethylpentane) to (3-methylhexane+2,4-dimethylpentane). The K1 value of the gas in the Donghe sandstone and the Jurassic reservoir is relatively consistent, ranging from 1.03 to 1.16 (Table 4; Fig. 9), indicating that the natural gas in the Donghe sandstone and the Jurassic reservoirs originated from the same source rocks.

The Donghe sandstone reservoir hosts a marine hydrocarbon and originates from Є–O source rocks in the southern study area, the Manjiaer Depression (Zhang et al., 2000, 2002; Chang et al., 2013; Zhu et al., 2013; Cheng et al., 2016; Huang et al., 2016). This indicates that the Donghe sandstone reservoir has a typical allogenic and far-source accumulation. The condensate reservoirs in the Tabei Uplift can be divided into the continental-facies and marine-facies ones. The former is characterized by the heavy value of the carbon isotope of ethane (–25.4 to –22.05‰); the values of Pr/Ph are more than 2, and both the values of Pr/nC_{17} and Ph/nC_{18} are less than 0.2. In contrast, the latter is characterized by a low value of the carbon isotope of ethane (–28 to –37‰); the value of Pr/Ph is less than 1.2, and both the values of Pr/nC_{17} and Ph/nC_{18} are more than 0.2 (Liang et al., 1998; Zhang et al., 2010; Liu et al., 2012). The values of Pr/Ph are less than 1, and both the values of Pr/

Table 1. **The oil properties and bulk composition of the Carboniferous Donghe sandstone and the Jurassic rocks**

Strata	Well	Well test results	Depth, m	Re + Asp, %	Wax, %	Sul,%	Viscosity 50 °C, mPa·s	Density 20 °C, g/cm^3	Sat, %	Aro, %	Re, %	Asp, %	Sat/Aro
Donghe Sandstone	DH1	Oil	5726–5746	11.7	4.8	0.7	6.9	0.863					
			5756–5800	11	7.6	0.7	5.7	0.858	60.2	18.8	12.8	7.9	3.2
			5810–5819	12.2	5.25	0.9	12.47	0.882					
	DH1-5-8	Heavy oil	5821–5839	42.53	14.21	1.86	4700	0.9202	–	–	–	–	–
	DH11	Oil	5712–5724	25.1	11.9	n.d.	5.6	0.858	53.7	21	5.3	4.4	2.56
		Condensate oil	5728–5739	–	–	–	–	0.763	–	–	–	–	–
	DH13	Heavy oil	5830.0–5858.5	–	–	–	–	–	–	–	–	–	–
		Bitumen	5871–5886	–	–	–	–	–	–	–	–	–	–
	DH1-H4	Oil	5835–6250	11.1	5.3	0.42	6.71	0.8569	39.9	5.8	5.4	47.5	6.9
	DH1-H5	Oil	5864–6365	8.48	9.39	0.66	6.939	0.8552	65.8	17.8	7.7	6.7	2.6
	DH1-7-9	Oil	5767–5802	12.45	11.67	0.84	13.29	0.8746	40.1	17.5	8.1	32.6	2.3
	DH1-H18c	Oil	5981–6016	7.77	6.2	0.78	6.227	0.8707	48.2	15.8	8.5	25.7	3.1
	DH1-H17	oil	5948–6348	9.41	4.99	0.71	6.955	0.8571	71.4	14.9	4.7	7	2.6
	DH20	Oil	5796–5810	13.8	5.8	0.9	15.2	0.885	–	–	–	–	–
		Heavy oil	5958–5970	29.1	n.d.	n.d.	5617.11	0.9813	–	–	–	–	–
	DH4	Oil	6068–6085	6.5	5.8	0.7	6	0.85	38.8	17.8	14.5	27.9	2.2
J_{IV}	DH20	Condensate oil	5480–5490	n.d.	6.4	n.d.	1.47	0.8172	45.62	16.06	8.03	28.49	2.84
	DH1-5-5	Oil	5483–5488	12.42	7.8	0.8	13.34	0.8769	25	15.67	11.67	47.33	1.6
	DH12	Condensate oil	5483–5491	4.87	3.15	0.24	1.3	0.7994	–	–	–	–	–
J_{III}	DH11	Heavy oil	5440–5450	n.d.	n.d.	n.d.	374.7	0.9478	–	–	–	–	–
	DH20	Condensate oil	5439–5443	0.5	2	1	0.83	0.7651	–	–	–	–	–
		Heavy oil	5446–5454	n.d.	n.d.	n.d.	5600	0.9814	25.57	25.28	8.81	39.78	1.01
	DH23	Condensate oil	5436.7–5445.0	n.d.	n.d.	n.d.	1.18	0.8023	–	–	–	–	–

Note. Re, Resin; Asp, asphaltene; Sul, sulfur; Sat, saturated hydrocarbons; Aro, aromatic hydrocarbons; Sat/Aro, the ratio of saturated to aromatic hydrocarbons; n.d., not determined; dash means there is no test data.

nC_{17} and Ph/nC_{18} are more than 0.2 in crude oil, heavy oil, asphaltic sand, and oil sand in the Donghe sandstone and the Jurassic reservoirs. This indicates that the hydrocarbon in the Donghe sandstone and the Jurassic reservoirs originate from the same source rocks.

Wang et al. (2008) suggested that, when i/nC_4 is less than 0.9, gas could form in three different conditions: The gas is mixed from liquid hydrocarbon cracking and kerogen degradation in a closed system when $i/nC_5 < 0.6$, from hydrocarbon cracking when i/nC_5 ranges from 0.6 to 0.85, and from kerogen degradation when $i/nC_5 > 0.85$. Since i/nC_4 in the Donghe sandstone and Jurassic reservoirs is less than 0.9, and i/nC_5 is between 0.39 and 0.91 in the Donghe sandstone reservoir and less than 0.6 in the Jurassic reservoir (Table 4), the gases in the Donghe sandstone reservoir are derived from both kerogen degradation and liquid hydrocarbon cracking, and the gases in the Jurassic reservoir are derived from liquid hydrocarbon cracking.

Time–space collocation between the fault mesh and hydrocarbon generation

Detailed hydrocarbon accumulation periods of the Carboniferous Donghe sandstone and Jurassic reservoirs in the Tabei Uplift were described by Zhang et al. (2012), Wang et al. (1997), and Zhang et al. (2006). Based on an integrated analysis of the previous research and the same source rocks of the Donghe sandstone and the Jurassic reservoir, we supposed that there were four stages of hydrocarbon charge of the clastic rock reservoir. The first stage occurred during the late Permian–Early Triassic with oil charge; the second stage occurred during the Late Jurassic–Late Cretaceous (151–85.8 Ma) with oil charge; the third stage occurred during the Eocene (50–40 Ma); and the fourth stage occurred during the Miocene (20 Ma) to present day with a gas charge.

Table 2. **The geochemical parameters of the Donghe sandstone and the Jurassic reservoirs**

Strata	Well	Sample type	Depth, m	Max peak	CPI	OEP	$\sum C_{21}$-/$\sum C_{22}$+	Pr/nC_{17}	Ph/nC_{18}	Pr/Ph	Carbon chain range
Donghe sandstone	DH1	Oil	5766.5	14	0.89	1.05	5.18	0.32	0.42	1	C_{12}–C_{34}
		Oil	5792	17	0.99	1.27	2.32	0.34	0.4	0.87	C_{13}–C_{30}
		Oil	5802	14	1.05	1.01	1.61	0.34	0.41	0.89	C_{11}–C_{34}
		Oil	5811.5	19	1.08	1.06	1.34	0.34	0.4	0.81	C_{12}–C_{35}
		Oil	5815.5	19	0.99	1	0.85	0.32	0.41	0.49	C_{13}–C_{36}
		Oil	5825	21	1	1	1.08	0.31	0.38	0.82	C_{13}–C_{35}
	DH1-H17	Oil	5948–6348	21	1.05	1.04	1.35	0.31	0.41	0.71	C_{10}–C_{36}
	DH20	Oil	5699.3	26	0.99	0.99	0.17	0.56	0.53	0.65	C_{15}–C_{38}
		Oil	5704.6	31	1.01	1	0.11	0.89	0.69	0.57	C_{16}–C_{38}
	DH1-H4	Oil	5835–6240	20	0.98	1	0.85	0.24	0.42	0.32	C_{11}–C_{36}
	DH1-6-8	Oil	5726–5809	21	1.08	1.06	1.22	0.32	0.42	0.7	C_{10}–C_{36}
	DH1-7-6	Oil	5483–5488	19	1.02	1.01	1.38	0.38	0.41	0.83	C_{14}–C_{36}
	DH1-7-9	Oil	5767–5802	18	1.09	1	1.62	0.35	0.43	0.8	C_{11}–C_{38}
	DH4	Oil	6068–6085	19	1.05	1.05	1.39	0.36	0.36	0.72	C_{15}–C_{36}
	DH6	Oil	5985–5998	19	1.03	1.04	1.16	0.4	0.46	0.78	C_{14}–C_{37}
J_{IV}	DH20	Oil	5480–5490	19	1.03	1.04	1.16	0.4	0.46	0.78	C_{14}–C_{37}
	DH1-5-5	Oil	5483–5488	19	1.03	1.04	1.16	0.4	0.46	0.78	C_{14}–C_{37}
J_{III}	DH30	Asphaltic sand	5418.9	20	1.03	0.96	0.86	0.24	0.42	0.33	C_{11}–C_{36}
		Asphaltic sand	5417.5	19	0.96	0.99	1.04	0.24	0.36	0.44	C_{10}–C_{36}
		Oil	5424–5426	20	1.1	0.93	1.19	0.31	0.48	0.47	C_{10}–C_{32}
	DH20	Heavy oil	5444–5451	17	1.04	n.d.	0.95	0.31	0.38	0.83	C_{15}–C_{37}
	DH1	Oil sand	5453	19	1	1.06	2.41	0.39	0.38	0.91	C_{13}–C_{35}
		Oil sand	5455	18	0.91	0.96	2.77	0.41	0.39	0.92	C_{13}–C_{35}
		Oil sand	5465	19	1.11	1.25	2.32	0.39	0.4	0.98	C_{12}–C_{35}

Note. N.d., Not determined.

Table 3. **The components of natural gas of the Donghe sandstone and the Jurassic rocks**

Strata	Well	Depth, m	C_1, %	C_{2+}, %	CO_2, %	N_2, %	C_1/C_{1+}, %	Relative density
Donghe sandstone	DH1	5726–5746	39.87	18.7	18.23	21.61	68.1	1.066
		5756–5800	43.92	15.46	19.35	20.98	74	1.009
	DH11	5712–5724	36.98	12.31	26.76	23.95	75	0.805
	DH6	5985–5998	28.88	20.04	23.21	27.87	59.1	1.18
	DH14	6116–6126	23.54	18.48	22.57	35.41	56	1.2
	DH4	6068–6086	23.83	25	20.38	30.64	48.8	1.22
	DH1-5-5	5745–5795	43.24	10.22	22.24	24.3	80.9	0.98
	DH1-H18c	5981–6016	34.5	7.8	31.1	26.6	81.6	1.049
J_{IV}	DH20	5480–5490	82.59	11.24	1.75	4.42	88	0.68
J_{III}	DH23	5443–5448	83.6	9.84	2.35	3.28	89.5	0.69
	DH20-H3	5542–6073	86.4	8.67	2.08	2.81	90.9	0.65

Note. C_1, Methane; C_{2+}, ethane and its heavier components; C_{1+}, total hydrocarbon components.

Table 4. **The light hydrocarbon parameters of natural gas of the Donghe sandstone and the Jurassic rocks**

Strata	Well	Depth, m	a, %	b, %	c, %	d, %	e, %	f	g	k_1	m	n
Donghe sandstone	DH1-H4	5835–6240	46.2	30.5	10.4	4.02	1.77	2.56	0.79	1.03	0.26	0.59
	DH1-H5	5864–6365	51.8	25.7	14.3	0.07	0.64	5.33	1.27	1.06	0.38	0.63
	DH1-6-8	5726–5809	50.0	27.4	2.6	0.18	0.91	4.98	1.37	1.08	0.37	0.67
	DH1-7-9	5767–5802	48.9	23.8	1.8	0.07	0.33	4.09	1.06	1.12	n.d.	0.47
	DH1-H17	5948–6348	45.1	19.5	2.1	0.12	0.63	4.86	1.22	1.13	0.39	0.68
	DH6	5985–5998	34.2	12.0	3.8	11.58	4.49	5.6	1.39	1.13	n.d.	0.39
	DH4-3	6082–6086	21.7	16.4	0.6	0.12	0.12	1.09	0.25	1.10	0.83	0.91
J_{IV}	DH20	5480–5490	46.37	33.79	9	3.36	4.44	3.89	1.01	1.07	0.49	0.5
	DH1-5-5	5483–5488	39.04	33.27	14.7	4.02	1.77	2.56	0.79	1.03	0.59	0.54
J_{III}	DH20-H1	5650–5973	37.27	26.21	18.9	4.38	13.18	5.85	1.35	1.12	0.42	0.39
	DH30	5424–5426	48.75	35.82	11.04	0.08	0.21	4.17	1.12	1.11	0.46	0.56
	DH20	5444–5451	45.18	32.31	16.07	2.5	3.92	3.53	0.92	1.16	0.7	0.59

Note. Definitions of compositions: a, *n*-alkanes; b, branched alkanes; c, cycloalkanes; d, benzene; e, toluene; f, 2-methylhexane; g, 2,3-dimethylpentane; k_1, (2-methylhexane + 2,3-dimethylpentane)/(3-methylhexane + 2,4-dimethylpentane); m, isopentane/*n*-pentane; n, isohexane/*n*-hexane.

Faults serve as the main unit in the source network. During faulting they acted as conduits for hydrocarbon migration; during the static stage, they acted as barriers (Hooper, 1991; Knipe, 1997; Indrevær et al., 2014). The active faults during the hydrocarbon generation stage can be conduits for hydrocarbon migration. The faults that formed after the hydrocarbon generation stage are significant for petroleum accumulation in the petroleum accumulation network and hydrocarbon adjustment of the transient storage reservoirs. The faults that formed before hydrocarbon generation are barriers to hydrocarbon migration.

According to the time–space collocation between the fault and hydrocarbon generation (Fig. 10), the F1 and F5 faults were active for the longest time and correlate well with four periods of hydrocarbon generation. The faults also connected two transient storages of the Donghe sandstone and J_{IV} braided river deposits, and they constitute the fully connected hydrocarbon source network with an unconformity between Jurassic and older strata. The F2, F3, F4, F9, F10, F11, and F12 faults form the low-connection hydrocarbon source network and only connect the Donghe sandstone and Ordovician source rocks. According to the relationship between the faulting and hydrocarbon generation stages of the F6, F7, and F8 faults, these faults transported the hydrocarbon to the Donghe sandstone transient storage traps during the structure inversion period.

The extensional faults that formed during the Eocene–Miocene and cut Triassic strata help with the migration of the hydrocarbon that accumulated in the J_{IV} transient storage to the J_{III} petroleum accumulation network. The faults can also serve as a minor hydrocarbon source network with a fully connected hydrocarbon source network that transports the hydrocarbon generated during the Eocene–Miocene to the traps, and it accumulates.

The reservoir models of fault mesh petroleum plays in the study area

The reservoirs in the study area are typically allogenic and characterized by far-source accumulation, such that the reservoir forms only when hydrocarbon transported by faults and unconformities constitutes the hydrocarbon source network. The carrier system of the fault mesh demonstrates four styles according to the characteristics of fault mesh petroleum plays: fully connected style (Fig. 11*a*), fault–unconformity–transient storage relay style (Fig. 11*b*), fault–transient storage–unconformity relay style (Fig. 11*c*), and transient

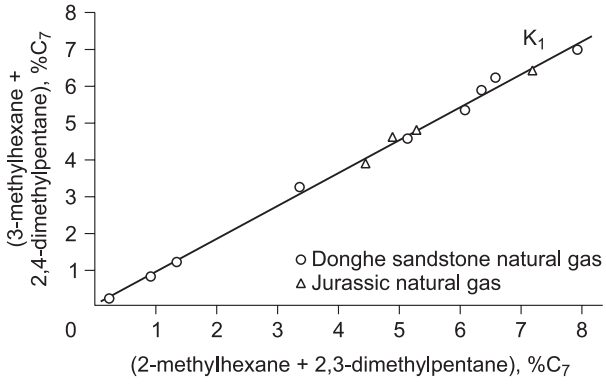

Fig. 9. Plot of (2-methylhexane+2,3-dimethylpentane) vs. (3-methylhexane+2,4-dimethylpentane).

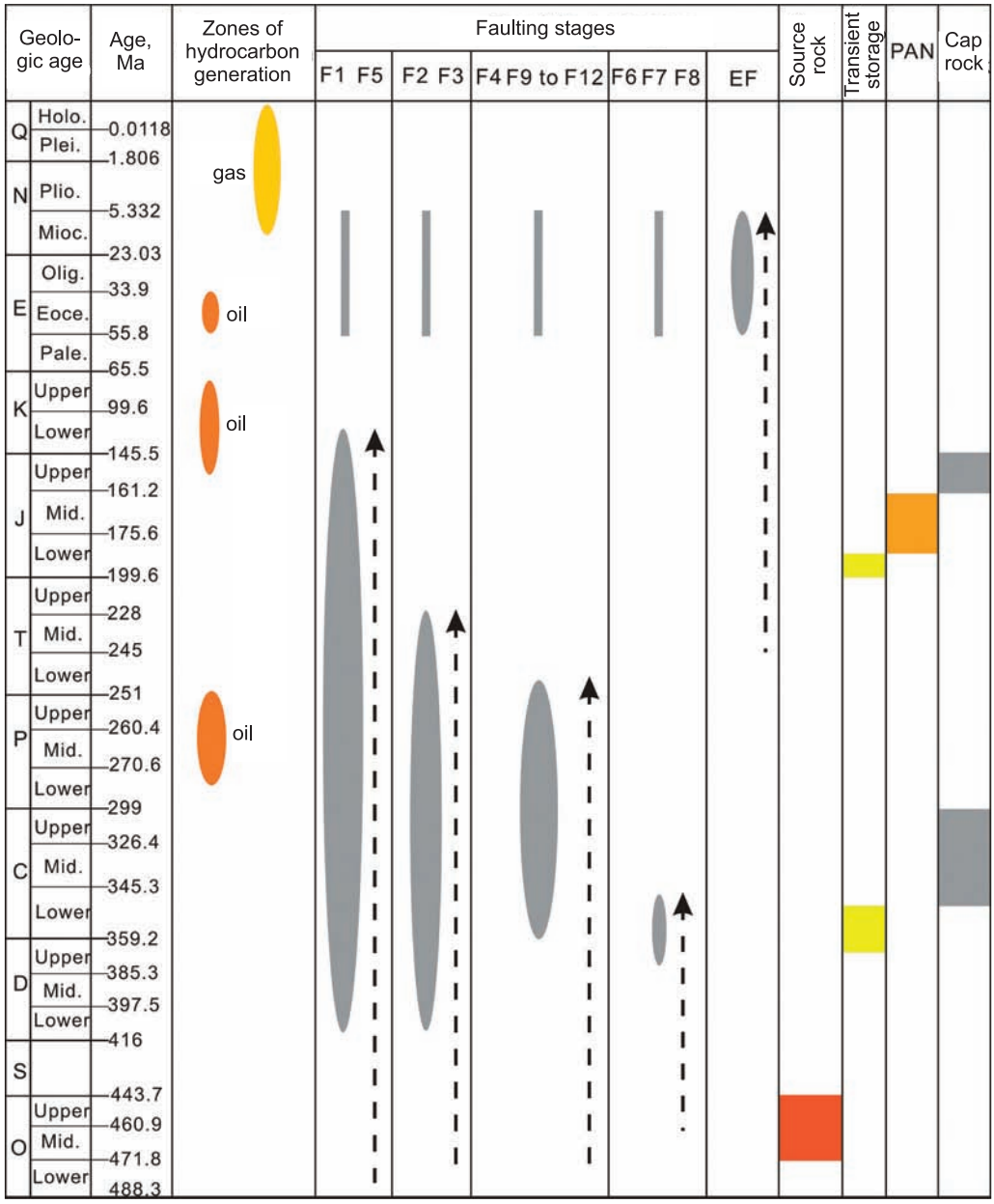

Fig. 10. The time–space collocation between the hydrocarbon generation and fault mesh. The fault numbers and locations are shown in Fig. 1, D.

EF, Extensional faults in the Jurassic; PAN, petroleum accumulation network. The dashed line with arrows is the strata that the faults cut; the gray solid line is the thrust fault that was reactivated during tectonic inversion. The ellipse is the faulting stage. Mid., Middle; Pale., Paleocene; Eoce., Eocene; Olig., Oligocene; Mioc., Miocene; Plio., Pliocene; Plei., Pleistocene; Holo., Holocene.

storage–fault relay style (Fig. 11*c*). Integrating the fault mesh characteristics and spatial relationships between the reservoir and transient storage, the reservoirs related to the fault mesh can be divided into inner-, upper-, and margin-transient storage reservoirs (Fig. 12).

The model of upper-transient storage reservoirs

Upper-transient storage reservoirs are located in the upper transient storage, which is a reservoir in the petroleum accumulation network that includes drape anticline, fault-block, and stratigraphic reservoirs (Fig. 12*a–c*). The carrier system is marked by a transient storage–fault relay style. The hydrocarbon that accumulated in the transient storage migrated along faults to the traps in the petroleum accumulation network. The

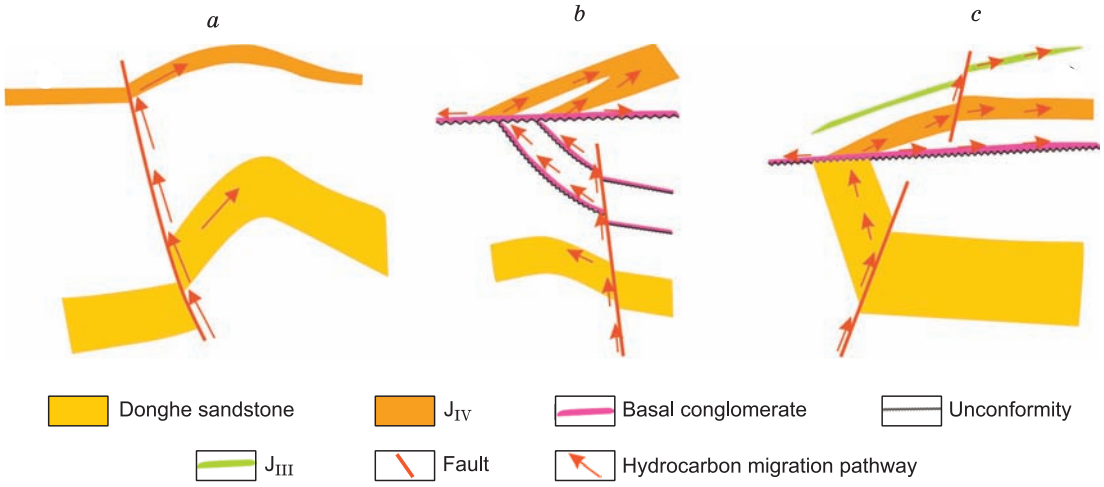

Fig. 11. The carrier system style of the fault mesh in the study area.

Upper-Transient Storage	Reservoir Model	a	b	c	d
	TrapType	Fault Block Traps	Lithologic Traps	Drape Anticline Traps	Lava-shielded Traps
	Potential Strata	J_{III} J_{2-3} K	J_{III} J_{2-3} K	J_{III}	P T
	Typical Well	DH12	DH4-6	DH20	Not found yet
Inner-Transient Storage	Reservoir Model	e	f	g	h
	TrapType	Fault Block Traps	Fault Anticline Traps	Fault Anticline Traps	Lithologic Traps
	Potential Strata	Donghe sandstone J_{IV}	Donghe sandstone	Donghe sandstone	J_{IV}
	Typical Well	Not found yet	DH6	DH1	DH1-5-5
	Reservoir Model	i	j	k	
	TrapType	Drape Anticline Traps	Lava-shielded Traps	CLT	
	Potential Strata	J_{IV}	Donghe sandstone	J_{IV}	
	Typical Well	DH20	Not found yet	Not found yet	
Margin-Transient Storage	Reservoir Model	l	m	n	o
	TrapType	Buried Hill Traps	Truncation Traps	Erosional Remnant	Lithologic Traps
	Potential Strata	Pre-Silurian	Donghe sandstone	J_{IV}	J_{IV}
	Typical Well	Not found yet	Not found yet	DH12	Not found yet

Mudstone, Buried hill, Limestone, Sandstone, Reservoirs, Igneous rock, Unconformity, Basal conglomerate, Fault

CLT: Channelized Lithologic Traps

Fig. 12. The reservoir models in the study area.

lava-shielded reservoir may exist because of strong volcanic activity during the Permian–Early Triassic (Liu et al., 2012).

The model of inner-transient storage reservoirs

Inner-transient storage reservoirs are located in the interior transient storage and are mainly anticline (Fig. 12*f, g, i*) and fault-block reservoirs (Fig. 12*e*). Lava-shielded reservoirs may exist in the transient storage of the Donghe sandstone. Stratigraphic reservoirs, such as sandbank lens (DH1-5-5 well), updip pinch-out sandstone, and channelized sandstone reservoirs (Fig. 12*k*), may exist in the transient storage of the J_{IV} braided river deposits (Fig. 12*h*). Here, hydrocarbon migrated in a fully connected hydrocarbon source network style (Fig. 11*a*), a fault–unconformity–transient storage relay style (Fig. 11*b*), or a fault–transient storage–unconformity–transient storage relay style (Fig. 11*c*) to the transient storage traps and accumulated.

The model of margin-transient storage reservoirs

Margin-transient storage reservoirs are located in the margin of the transient storage and are mainly related to the unconformity. There are three layers in the unconformity complex, including the rocks above the unconformity interface, a weathered clay and paleokarst zone, and different compositions that can form different reservoir types (Martinsen, 2003a,b; He et al., 2007). Simulation experiments show that weathered clay is the key part in the formation reservoirs for the unconformity-related hydrocarbon reservoirs (Wu et al., 2009). According to the stratigraphic contact relationships, the reservoirs related to the regional unconformity between the Jurassic and older strata were divided into buried-hill (Fig. 12*l*), truncate (Fig. 12*m*), erosional-remnant (Fig. 12*n*), and stratigraphic reservoirs (Fig. 12*o*), where the sandstone fills up a local low in the paleotopography.

The truncate reservoirs may not exist in the study area, because the basal conglomerate above the unconformity interface between Jurassic and Carboniferous is 3 to 5 m thick, which is widely distributed, according to well data (Fig. 7). The failed DH2 and DH3 exploration wells that tested the unconformity reservoir also indicate that the targets are high-risk ones. The drilling results for well DH22 show that a thick lacustrine mudstone sits above the unconformity interface between Jurassic and pre-Carboniferous, meaning that buried-hill reservoirs may exist in the study area. Erosional remnants were formed by differential weathering in the Jurassic strata, and the hydrocarbon migrated to the traps in a fault–unconformity relay style, such as the DH12 reservoir in the Jurassic.

The process of fault mesh petroleum plays from Carboniferous to Jurassic in the study area

Based on an integrated analysis of the faulting and hydrocarbon generation, there are four periods of hydrocarbon generation and multiple hydrocarbon reservoirs adjustments. Below, the DH1 oilfield is used as an example to elaborate on the formation of fault mesh reservoirs. Three times hydrocarbon-charged history can be concluded following Zhang et al. (2012) and Zhang and Luo (2012), who used the homogenization temperature of salt-water inclusions associated with hydrocarbon inclusions in the DH11 well and K–Ar dating of authigenic illite of Devonian sandstone reservoirs in the Ha 6 well from the Halahatang sag, respectively (Fig. 13). The timing of hydrocarbon charging is as follows: the late Permian to Early Triassic, charged with hydrocarbon oil; the Jurassic to Cretaceous, charged with hydrocarbon oil; and the Late Neogene, charged with hydrocarbon gas originated from underlying liquid hydrocarbon cracking and kerogen degradation (Zhang et al., 2002; Zhu et al., 2013b; Lei et al., 2019), in which we divided it into two subperiods according to the time–space collocation between the fault mesh and hydrocarbon generation (section 5.2).

The first stage (Permian to Triassic)

The hydrocarbon originated from an Ordovician source rock in the southern study area of the Manjiaer Depression, migrated along a hydrocarbon source network to the Donghe sandstone traps, and accumulated. The Donghe sandstone in the north was uplifted to the surface during intensive compressive deformation in the Permian–Triassic (Fig. 13*g, h*) and was directly connected with fresh water. Thus, the reservoir formation period was simultaneous with the accumulation of hydrocarbons, which experienced water washing and biodegradation. The bitumen formed near the unconformity interface and the partial reservoir at the base of the Donghe sandstone reservoirs underwent long-term biodegradation (Fig. 13*d*), and bitumen exists in the DH13 well (Table 1), located in the saddle. There was strong volcanic activity during the Permian–Triassic; we suggest that the high contents of CO_2 and N_2 in the Donghe sandstone reservoir were due to volcanic degassing.

The second stage (Jurassic to Cretaceous)

The Jurassic–Cretaceous stage can be divided into two substages based on the hydrocarbon generation periods. In the first substage, during J_{1-2} before hydrocarbon generation, the hydrocarbon reservoirs that accu-

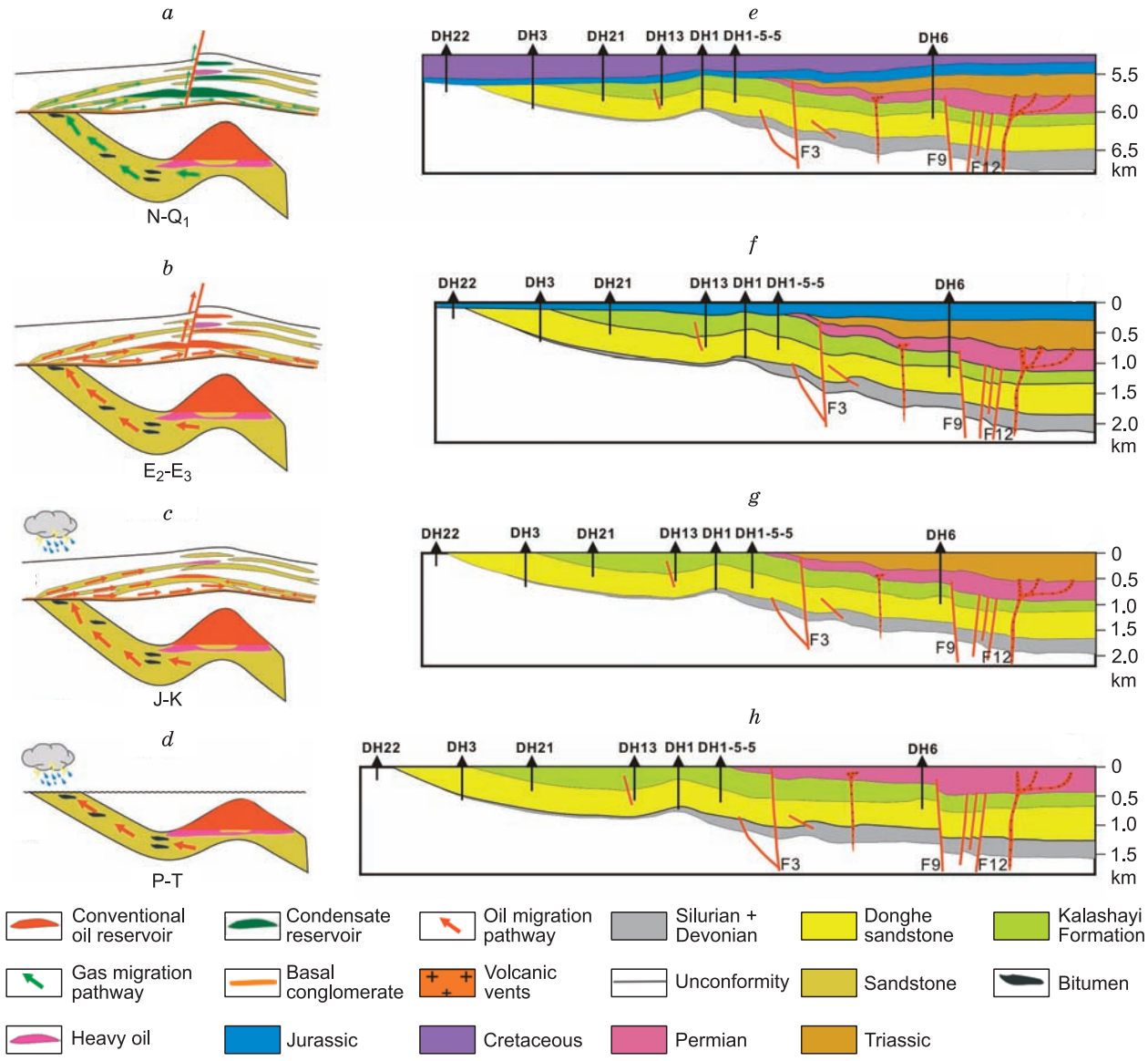

Fig. 13. The hydrocarbon accumulation process of fault mesh petroleum plays in the study area. The well locations and fault numbers are shown in Fig. 1, D.

mulated in the transient storage of the Donghe sandstone during the Permian–Triassic migrated through a fully connected hydrocarbon source network along fault F5 to the Jurassic traps. The second substage was the J_3–Cretaceous hydrocarbon generation period. The hydrocarbon migrated in a transient storage–unconformity and fault–unconformity relay style to the Donghe sandstone transient storage traps, J_{IV} braided river deposits transient storage traps, and J_{III} alluvial fan petroleum accumulation network and accumulated (Fig. 13*c*). The Jurassic strata were then buried to a depth shallower than 500 m in this stage (Fig. 13*f*), a depth conducive to biodegradation. The heavy oil from the Jurassic reservoirs formed in this stage.

The third stage (Eocene)

The thrust faults in the Paleozoic were reactivated during inversion. The hydrocarbon generated in this stage migrated in a fully connected hydrocarbon source rocks style, fault–transient storage–unconformity relay style, and fault–unconformity–transient storage relay style to the traps in the transient storage of the Donghe sandstone, and J_{IV} braided river deposits and petroleum accumulation network of the J_{III} alluvial fan deposits and accumulated to form a reservoir (Fig. 13*b*). The normal oil in the Jurassic reservoirs accumulated in this stage.

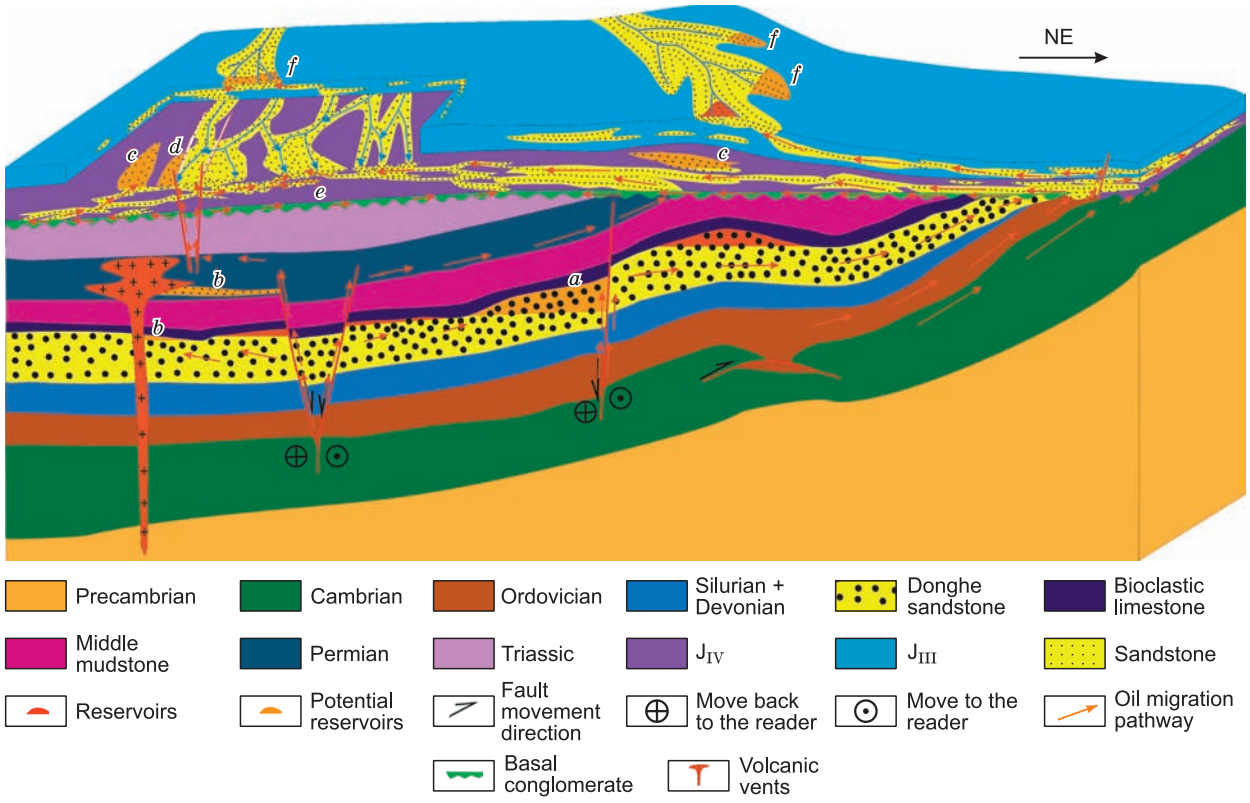

Fig. 14. The model of fault mesh petroleum plays in the study area, not to scale. See the text for additional details.

The fourth stage (Miocene)

The gaseous hydrocarbon charged in this stage originated from oil and kerogen cracking. Gas washing occurred in the earlier hydrocarbon reservoirs during gaseous hydrocarbon charging. The crude oil dissolved, and the light hydrocarbon fraction migrated to the traps through faults and the unconformity and formed condensate and light hydrocarbon (Silverman, 1985; Thompson, 1987, 1988; Meulbroek et al., 1998; Masterson et al., 2001). There is evidence of condensate reservoirs formed by gas washing in the Ordovician and Carboniferous reservoirs in the Tazhong and Tabei Uplifts, Tarim Basin (Zhu et al., 2013a, b; Chen et al., 2014). The gaseous hydrocarbon originated from the same source rock in the Donghe sandstone and the Jurassic reservoirs. This indicates that the gaseous hydrocarbon in the Jurassic reservoirs must have migrated through the lower part of the Donghe sandstone reservoirs, and in that process the Donghe sandstone reservoirs experienced gas washing. The light hydrocarbon fraction was formed by gas washing when it migrated along faults and the unconformity to the Jurassic traps and accumulated to form condensate reservoirs (Fig. 13*a*).

There are multiple periods of hydrocarbon accumulation and adjustment, and hydrocarbons migrated and accumulated in a fault mesh style to the clastic rock reservoirs in the study area. The transient storage of the Carboniferous Donghe sandstone was connected with the transient storage of the J_{IV} formation in different fault mesh types (Fig. 11). The hydrocarbon that originated from the Ordovician source rocks of the southern Manjiaer Depression temporarily accumulated in the transient storage of the Donghe sandstone during the Permian–Triassic. The hydrocarbon that accumulated in the transient storage of the Donghe sandstone experienced gas washing and formed a light hydrocarbon fraction during the Jurassic–Miocene. These hydrocarbons migrated along a fault mesh, adjusted to the Jurassic transient storage and petroleum accumulation network, and accumulated in the Jurassic traps, forming secondary condensate reservoirs in the Jurassic.

The hydrocarbon exploration significance of the fault mesh petroleum plays in the study area

There are two different sedimentary origins of the transient storage units in the study area, which determined the different exploration targets in the Carboniferous Donghe sandstone and the Jurassic rocks. The main

target in the shoreline deposits of the Donghe sandstone is fault-related reservoirs because of the lack of mudstone. Faults are a three-dimensional geologic bodies with a complex architecture (Chester et al., 1993; Caine et al., 1996; Childs et al., 1997; Aydin, 2000; Yielding et al., 2010), and the faults with sandstone self-juxtaposition can seal laterally through fault rocks and deformation bands (Fossen and Bale, 2007; Fossen et al., 2007, 2011; Faulkner et al., 2010; Tueckmantel et al., 2010). We suggest that deformation band clusters seal some faults in the study area, following an integrated analysis of the original formation fluids and faulting mechanisms, and formed fault-block reservoirs (Fig. 14*a*). The discussion of sandstone self-juxtaposition faults closure is beyond the scope of this study. The lava-shielded reservoirs may exist in the transient storage of the Donghe sandstone because of volcanic activity during the Permian–Triassic (Fig. 14*b*).

The exploration target related to the inner- and upper-transient storage can be found in the Jurassic. For the J_{IV} braided river deposits of transient storage, the channelized lithologic related reservoirs (Fig. 14*c*) and sandbank lenses stratigraphic-related reservoirs (Fig. 14*d*) are present owing to the migration of channels, and fault-block reservoirs related to the channel sandstone and faults (Fig. 14*e*). The J_{III} formation is an alluvial-fan depositional system as a petroleum accumulation network, the related of upper-transient storage reservoirs can be found with the composition of J_{IV} braided river deposits, such as stratigraphic-related reservoirs for the fast change of rock facies (Fig. 14*f*).

CONCLUSIONS

(1) There are four periods of hydrocarbon charging, with oil charging during the first three periods and gas charging during the last. These periods are characteristic of reservoir formation with fault mesh migration and accumulation in the clastic rock reservoirs in the Donghetang area, Tabei Uplift, Tarim Basin, northwestern China. The hydrocarbon accumulation process of fault mesh petroleum plays is the key reason why there are multistrata reservoirs in the study area, but each has different hydrocarbon properties;

(2) There are two sets of fault meshes in the study area: the Donghe sandstone and Permian and Triassic strata combination as well as the J_{IV} and J_{III} formation combination in the Jurassic strata;

(3) The hydrocarbons of the Donghe sandstone and Jurassic reservoirs originate from the same source rocks, marine hydrocarbon from the southern Manjiaer Depression. The reservoirs of the Jurassic have a light hydrocarbon fraction that originated from gas washing of the Donghe sandstone reservoirs, migrated in a different carrier system style to the Jurassic traps, and formed secondary condensate reservoirs;

(4) The reservoirs in the Donghetang area are typical allochthonous and far-source fault mesh petroleum plays. The highly effective hydrocarbon carrier system is key to hydrocarbon accumulation.

(5) The hydrocarbon carrier system in the fault mesh petroleum plays in the study area can be divided into fully connected, fault–unconformity–transient storage relay, fault–transient storage–unconformity relay, and transient storage–fault relay styles according to the architecture of the fault mesh. The different compositions of the fault mesh units can form three categories (upper-, inner-, and margin-transient storage reservoirs) and 15 types of reservoirs.

The authors are thankful for permission of Tarim Oilfield Company to publish this paper. We acknowledge data contribution and sample collection from the Research Institute of Petroleum Exploration and Development in Tarim Oilfield Company, PetroChina. This research was funded by the National Science and Technology Major Project (No. 2017ZX05001) in China. We are grateful to editors and anonymous reviewers for very constructive and useful comments.

REFERENCES

Aydin, A., 2000. Fracture, faults, and hydrocarbon entrapment migration and flow. Mar. Pet. Geol. 7 (17), 797–814.

Caine, J.S., Evans, J.P, Forster, C.B, 1996, Fault zone architecture and permeability structure. Geology 24, 1025–1028.

Chang, X.C., Wang, T.G., Li, Q.M., Cheng, B., Zhang, L.P., 2013. Geochemistry and possible origin of petroleum in Palaeozoic reservoirs from Halahatang Depression. J. Asian Earth Sci. 47, 129–141.

Chen, C.M., Lu, H.F., Wang, G.Q., Jia, D., Cai, D.S., 1998. Analyses of superimposed structures in the north Tarim Uplift, Tarim Basin [in Chinese with English abstract]. Geological Journal of China Universities, 4 (3), 294–302.

Chen, J.Q., Pang, X.Q., Jiang, Z.X., Pang, H., 2014. Controlling factors and phase state of hydrocarbons in the upper Ordovician of the Tazhong area, Tarim Basin [in Chinese with English abstract]. Nat. Gas Geosci., 25 (12), 1913–1924.

Cheng, B., Wang, T.G., Chen, Z.H., Chang, X.C., Yang, F.L., 2016. Biodegradation and possible source of Silurian and Carboniferous reservoir bitumens from Halahatang sub-depression, Tarim Basin, NW China. Mar. Pet. Geol. 78, 236–246.

Cheng, H.Y., Li, J.H., Zhao, X., 2009. The structural styles of different structural layers in the western part of north Tarim Uplift and their genetic mechanisms [in Chinese with English abstrat]. Geol. J. China Univ. 15 (4), 529–536.

Chester, F.M., Evans, J.P., Biegel, R.L., 1993. Internal structure and weakening mechanisms of the San Andreas fault. J. Geophys. Res. Solid Earth 98 (1), 771–786.

Childs, C., Watterson, J., Walsh, J.J., 1996. A model for the structure and development of fault zones. J. Geol. Soc. London 153, 337–340.

Demaison, G., 1984. The generative basin concept, in: Demaison, G., Murris, R.J. (Eds.), Petroleum geochemistry and basin evaluation. AAPG Mem. 35, 1–14.

Dow, W.G., 1972. Application of oil correlation and source rock data to exploration in Williston Basin (abs.). AAPG Bull. 56, 615.

Dow, W.G., 1974. Application of oil correlation and source rock data to exploration in Williston Basin. AAPG Bull. 58 (7), 1253–1262.

Faulkner, D.R., Jackson, C.A.L., Lunn, R.J., Schlische, R.W., Shipton, Z.K., Wibberley, C.A.J., Withjack, M.O., 2010. A review of recent developments concerning the structure, mechanics and fluid flow properties of fault zones. J. Struct. Geol. 32 (11), 1557–1575.

Fossen, H., Schultz, R.A., Shipton, Z.K., Mair, K., 2007. Deformation bands in sandstone: a review. J. Geol. Soc. 164 (4), 755–769.

Fossen, H., Schultz, R.A., Torabi, A., 2011. Conditions and implications for compaction band formation in the Navajo Sandstone, Utah. J. Struct. Geol. 33 (10), 1477–1490.

He, D.F., Zhou, L., Tang, Y., Wu, X.Z., Du, S.K., 2007. Characteristics of unconformity between the Xishanyao Formation and Toutunhe Formation of the Middle Jurassic in Junggar Basin the its significance in petroleum exploration [in Chinese with English abstract]. J. Palaeogeogr., 9 (4), 387–395.

Hooper, E.C.D., 1991. Fluid migration along growth fault in compacting sediments. J. Pet. Geol. 14, 161–180.

Hu, C.Y., 1986. An approach on regional controlling factors of oil-gas field distribution in offshore sedimentary basins of China [in Chinese with English abstract]. Mar. Geol. 6 (4), 23–29.

Huang, H.P., Zhang, S.C., Su, J., 2016. Palaeozoic oil-source correlation in the Tarim Basin, NW China: A review. Org. Geochem. 94, 32–36.

Indrevær, K., Stunitz, H., Bergh, S.G., 2014. On Palaeozoic–Mesozoic brittle normal faults along the SW Barents Sea margin: fault processes and implications for basement permeability and margin evolution. J. Geol. Soc. 171 (6), 831–846.

Jin, Z.J., Wang, Q.C., 2004. New progresses in research of China's typical superimposed basins and preservation of hydrocarbons: taking the Tarim basin as an example [in Chinese]. Sci. China, Ser. D Earth Sci. 34 (Suppl. 1), 1–12.

Knipe, R.J., 1997. Juxtaposition and seal diagrams to help analyze fault seals in hydrocarbon reservoirs. AAPG Bull. 81 (2), 187–195.

Lei, Z.C., Xu, H.M., Jiang, T.W., Li, Z.C., Li, J.W., Li, W.L., Xiong, Y.B., Li, S.Z., Zhao, J.W., 2019. Multiple phase hydrocarbons from Carboniferous reservoir rocks and their origin in the Donghetang area, Western Tabei Uplift, Tarim Basin, NW China. Russ. Geol. Geophys. 60 (2), 215–230.

Li, D.S., Liang, D.G., Jia, C.Z., Wang, G., Wu, Q.Z., He, D.F., 1996. Hydrocarbon accumulation in the Tarim Basin, China. AAPG Bull. 80 (10), 1587–1603.

Li, W.L., Xu, H.M., Niu, Y.J., Wang, C., Gao, S.Y., 2016. Sand body types of clastic shore deposits with delta backgrounds and their control over reservoir quality. Arabian J. Geosci. 9, 247.

Liang, D.G., Gu, Q.Y., Pi, X.J., 1998. Distribution law of the condensate gas reservoir in Tabei Uplift [in Chinese with English abstract]. Nat. Gas Ind. 18 (3), 5–9.

Liu, Y.L., Huang, Z.B., Wu, G.Y., Wu, G.Y., Zhen, D.M., 2012. ^{40}Ar-^{39}Ar geochronology and geochemistry of the volcanic rocks from the west segment of Tabei Uplift, Tarim Basin [in Chinese with English abstract]. Acta Petrol. Sin. 28 (8), 2423–2434.

Magoon, L.B., 1988. The petroleum system — A classification scheme for research, exploration, and resource assessment, in: Magoon, L.B. (Ed.), Petroleum Systems of the United States. USGS Bull. 1870, 2–15.

Magoon, L.B., 1992. Identified petroleum systems within the United States—1992, in: Magoon, L.B. (Ed.), The Petroleum System — Status of Research and Methods, 1992. USGS Bull. 2007, 2–11.

Magoon, L.B., Dow, W.G., 1994. The petroleum system: From source to trap. AAPG Mem. 60, 3–24.

Mango, F.D., 1987. An invariance in the isoheptanes of petroleum. Science 273, 514–517.

Mango, F.D., 1990. The origin of light cycloalkanes in petroleum. Geochim. Cosmochim. Acta 54, 23–27.

Martinsen, R.S., 2003a. Depositional remnants, Part 1: Common components of the stratigraphic record with important implications for hydrocarbon exploration and production. AAPG Bull. 87 (12), 1869–1882.

Martinsen, R.S., 2003b. Depositional remnants, Part 2: Examples from the Western Interior Cretaceous basin of North America. AAPG Bull. 87 (12), 1883–1909.

Masterson, W.D., Dzou, L.I.P., Holba, A.G., Fincannon, A.L., Ellis, L., 2001. Evidence for biodegradation and evaporative fractionation in West Sak, Kuparuk and Prudhoe Bay field areas, North Slope, Alaska. Org. Geochem. 32 (3), 411–441.

Meissner, F.F., 1984. Petroleum geology of the Bakken Formation, Williston basin, North Dakota and Montana, in: Demaison, G., Murris, R.J. (Eds.), Petroleum Geochemistry and Basin Evaluation. AAPG Mem. 35, 159–179.

Meulbroek, P., Cathles, L., Whelan, J., 1998. Phase fractionation at South Eugene Island Block 330. Org. Geochem. 29 (1), 223–239.

Pang, X.Q., Jin, Z.J., Jiang, Z.X., Zuo, S.J., 2003. Evaluation of hydrocarbon resources of superimposed basin and its significance [in Chinese with English abstract]. Pet. Explor. Dev. 29 (1), 9–13.

Pang, X.Q., Zhou, X.Y., Lin, C.S., Huo, Z.P., Luo, X.R., Pang, H., 2010. Classification of complex reservoirs in superimposed basins of western China. Acta Geol. Sin. 84 (5), 1011–1034.

Perrodon, A., 1983. Dynamics of oil and gas accumulation. Bulletin des Centres de Recherches Exploration-Production. Elf-Aquitaine, Pau, pp. 187–210.

Perrodon, A., 1992. Petroleum systems: models and applications. J. Pet. Geol. 15 (3), 319–326.

Silverman, S.R., 1985. Migration and segregation of oil and gas. AAPG Bull., Mem. 4, 53–65.

Tang, L.J., Jin, Z.J., Zhang, Y.W., Lu, K.Z., 1999. Negative inversion structures and geological significance of northern Uplift, the Tarim Basin, NW China [in Chinese with English abstract]. Geoscience 13 (1), 93–98.

Tang, L.J., Qi, L.X., Qiu, H.J., Yun, L., Li, M., 2012. Poly-phase differential fault movement and hydrocarbon accumulation of the Tarim Basin, NW China [in Chinese with English abstract]. Acta Petrol. Sin. 28 (8), 2569–2583.

Thompson, K.F.M., 1987. Fractionated aromatic petroleums and the generation of gas-condensates. Org. Geochem. 11 (6), 573–590.

Thompson, K.F.M., 1988. Gas-condensate migration and the petroleum fractionation in deltaic systems. Mar. Pet. Geol. 5 (4), 237–245.

Tueckmantel, C., Fisher, Q.J., Knipe, R.J., Lickorish, H., Khalil, S.M., 2010. Fault seal prediction of seismic-scale normal faults in porous sandstone: a case study from the eastern Gulf of Suez rift, Egypt. Mar. Pet. Geol. 27 (2), 334–350.

Ulmishek, G., 1986. Stratigraphic aspects of petroleum resource assessment, in: Rice, D.D. (Ed.), Oil and Gas Assessment Methods and Application. AAPG Stud. Geol. 21, 59–68.

Wang, F.Y., He, P., Zhang, S.C., Zhao, M.J., Lei, J.J., 1997. The K-Ar isotopic dating of authigenic illites and timing of hydrocarbon fluid emplacement in sandstone reservoir [in Chinese with English abstract]. Geol. Rev. 43 (5), 540–546.

Wang, Y.P., Zhao, C.Y., Wang, Z.Y., Wang, H.H., Tian, J., Zou, Y.R., Liu, Z.Z., 2008. Identification of marine natural gases with different origin sources. Sci. China, Ser. D Earth Sci. 51 (Suppl. 1), 148–164.

Wang, Y.S., Li, M.W., Pang, X.Q., Zhang, S.W., Shi, D.S., Dong, X., 2005. Fault-fracture mesh petroleum plays in the Zhanhua Depression, Bohai Bay Basin: Part 1. Source rock characterization and quantitative assessment. Org. Geochem. 36, 183–302.

Wang, Z.M., Tian, J., Shen, Y.M., Zhou, L.X., Wang, Z.Y., 2004. Sedimentary facies of Donghe Sandstone during the late Devonian to Early Carboniferous in Tarim Basin [in Chinese with English abstract]. J. Palaeogeogr. 6 (3), 289–295.

Wei, G.Q., Jia, C.Z., Shi, Y.S., Lu, H.F., Li, Y.H., 2001. Tectonic characteristics and petroleum accumulation in extensional shear fault system in Mesozoic-Cenozoic Formations in the northern area of Tabei Uplift, Tarim Basin [in Chinese with English abstract]. Acta Petrol. Sin., 22 (1), 19–24.

Wu, K.Y., Li, L.L., Zha, M., 2009. Vertical structures of unconformity and its simulation experiment of hydrocarbon accumulation mechanism [in Chinese with English abstract]. Pet. Geol. Exp. 31 (5), 537–541.

Xu, H.M., Xu, Z.H., Zhang, S.W., Wang, Z.G., Wang, Y.S., 2008. Layer structure petroleum accumulation system and characteristic of subtle reservoir of continental basin in eastern China: Taking Jiyang Depression for example [in Chinese with English abstract]. Sci. China Ser. D Earth Sci. 38 (Suppl. 1), 129–137.

Yielding, G., Bretan, P., Freeman, B., 2010. Fault seal calibration: A brief review, in: Jolley, S.J., Fisher, Q.J., Ainsworth, R.B., Vrolijk, P.J., Delisle, S. (Eds.), Reservoir Compartmentalization. Geol. Soc. London Spec. Publ. 347, 243–255, doi:10.1144 /SP347.14.

Zhang, B., Cui, J., Gu, Q.Y., Zhu, G.Y., Su, J., 2010. Oil origin classification in composite hydrocarbon accumulation play in the western Tabei Uplift and its geological significance [in Chinese with English abstract]. Acta Petrol. Sin., 31(1), 55–67.

Zhang, B., Zhu, G.Y., Su, J., Lu, Y.H., 2012. Origin and distribution of hydrocarbon in Donghe Oilfield, west Tabei Uplift, Tarim Basin [in Chinese with English abstract]. Earth Sci. Front. 19 (4), 276–283.

Zhang, S.C., Hanson, D.G., Liang, D.G., Chang, E., Fago, F., Hanson, A.D., 2000. Paleozoic oil source rock correlation in the Tarim Basin, NW China. Org. Geochem. 31 (4), 273–286.

Zhang, S.C., Liang, D.G., Li, M.W., Xiao, Z.Y., He, Z.H., 2002. Molecular fossils and oil-source rock correlations in the Tarim Basin, NW China. Chin. Sci. Bull. 47 (S), 20–27.

Zhang, S.C., Zhang, B., Yang, H.J., Zhu, G.Y., Su, J., Wang, X.M., 2012. Adjustment and alteration of hydrocarbon reservoirs during the Late Himalayan Period, Tarim Basin, NW China. Pet. Explor. Dev. 9 (6), 668–680.

Zhang, S.W., Wang, Y.S., Shi, D.S., Xu, H.M., 2003. Fault-fracture mesh petroleum play: An example from the Neogene of the Jiyang Superdepression [in Chinese with English abstract]. Pet. Explor. Dev. 30 (1), 1–10.

Zhang, S.W., Wang, Y.S., Shi, D.S., Xu, H.M., Pang, X.Q., Li, M.W., 2004. Fault-fracture mesh petroleum plays in the Jiyang Superdepression of the Bohai Bay Basin, eastern China. Mar. Pet. Geol. 21, 651–668.

Zhang, S.W., Lin, H.X., Shen, Y., 2013. Analysis on meshwork-carpet pool-forming mechanism of Chepaizi Uplift and enlightenment on petroleum exploration of Junggar Basin [in Chinese with English abstract]. Geol. Rev. 59 (3), 489–500.

Zhang, Y.M., Wang, B., Ou, G.X., 2006. Research on Jurassic oil-gas accumulated period and order in Kongquehe region, Tarim Basin [in Chinese with English abstract]. Pet. Geol. Eng. 20 (5), 2–5.

Zhang, Y.Y., Luo, X.Q., 2012. K-Ar and Ar-Ar dating of authigenic illite and hydrocarbon accumulation history of Carboniferous and Silurian sandstone reservoirs in well Ha 6, Tarim basin [in Chinese with English abstract]. Acta Petrol. Sin. 33 (5), 748–755.

Zhao, W.Z., He, D.F., 2000. Concept and its significance of composite petroleum systems in China [in Chinese with English abstract]. Pet. Explor. 5 (3), 1–12.

Zhu, G.Y., Zhang, S.C., Su, J., 2013a. Secondary accumulation of hydrocarbons in Carboniferous reservoirs in the northern Tarim Basin, China. J. Pet. Sci. Eng. 102, 10–26.

Zhu, G.Y., Zhang, S.C., Su, J., Zhang, B., Yang, H.J., Zhu, Y.F., Gu, L.J., 2013b. Alteration and multi-stage accumulation of oil and gas in the Ordovician of the Tabei Uplift, Tarim Basin, NW China: Implications for genetic origin of the diverse hydrocarbons. Mar. Pet. Geol. 46, 234–250.

Поступила в редакцию 14 августа 2018 г.,
принята в печать 22 мая 2019 г.